The lateral periaqueductal gray and its role in controlling predatory hunting and social defense.

Ignacio Marín-Blasco
University of São Paulo / Institute of Biomedical Sciences
Miguel Rangel Jr.
University of São Paulo / Institute of Biomedical Sciences
Marcus Baldo
University of São Paulo / Institute of Biomedical Sciences
Simone Motta
University of São Paulo / Institute of Biomedical Sciences
Lisa Stowers
Scripps Research https://orcid.org/0000-0002-4403-1269
Newton Canteras (newton@icb.usp.br)
University of São Paulo / Institute of Biomedical Sciences https://orcid.org/0000-0002-7205-5372

Article

Keywords: prey hunting, social agonistic behavior, motivation

Posted Date: November 17th, 2020

DOI: https://doi.org/10.21203/rs.3.rs-103640/v1

The lateral periaqueductal gray and its role in controlling predatory hunting and social defense.

Authors: Ignacio Javier Marín-Blasco[1#], Miguel José Rangel Jr.[1#], Marcus Vinicius C. Baldo[2], Simone Cristina Motta[1], Lisa Stowers[3], Newton Sabino Canteras[1*].

[1]Dept. Anatomy, Institute of Biomedical Sciences, University of São Paulo; São Paulo, SP 05508-000, Brazil.

[2]Dept. Physiology and Biophysics, Institute of Biomedical Sciences, University of São Paulo; São Paulo, SP 05508-000, Brazil.

[3]Dept. of Cell Biology, The Scripps Research Institute, La Jolla, CA 92037, USA.

Number of words in abstract: 150; Number of words in manuscript: 4,411; Number of words in methods: 3,372; Number of figures: 5; Number of supplementary materials: 6

# Authors have equal contribution in the study

*Corresponding Author:
Newton Sabino Canteras, M.D., Ph.D.
Department of Anatomy,
Institute of Biomedical Sciences,
University of Sao Paulo,
Av. Lineu Prestes, 2415,
CEP 05508-000 São Paulo, SP, Brazil
Phone: +55.11.3091.7628 Fax: +55.11.3091.7285
e-mail: newton@icb.usp.br

Abstract

Evasion from imminent threats and prey attack are opposite behavioral choices critical to survival. The lateral periaqueductal gray (LPAG) is a key player in these behaviors, it responds to social threats and prey hunting while also driving predatory attacks and active defense. Our results revealed that distinct neuronal populations in the LPAG drive prey hunting and evasion from social threats. We show that the LPAG provides a putative glutamatergic projection to the lateral hypothalamic area (LHA). LPAG > LHA pathway optogenetic inhibition impaired insect predation but did not alter escape/attack ratio during social defeat. The results suggest that the LPAG control over evasion to a social attack may be regarded as a stereotyped response depending probably on descending projections. Conversely, the LPAG control over predatory behavior involves an ascending pathway to the LHA that likely influences LHA^{GABA} neurons driving predatory hunting and may provide an emotional drive for appetitive rewards.

Keywords – prey hunting, social agonistic behavior, motivation

Introduction

The periaqueductal gray (PAG) commonly has been recognized as a downstream site in neural networks for the expression of a variety of behaviors, for example, sexual, maternal, and defensive behaviors with accompanying modulation of nociceptive transmission, autonomic changes, and vocalization [1-9]. By and large, PAG-related responses have been regarded as being mostly stereotyped and dependent on descending projections to the lower brainstem and spinal cord. However, the PAG is also known to influence complex events like approach and avoidance responses to perform risk assessment of potential threats [10-13], fear memory processing [14-19], and reward-seeking [20-23].

It is particularly puzzling that the PAG controls both aversive and rewarding behaviors. In this regard, we call special attention to the lateral part of the PAG (LPAG) that has been implicated in mediating the opposite behavioral choices of predatory attack and evasion from a conspecific aggressor. Previous studies from our laboratory have associated the LPAG with the organization of prey hunting. Insect predation was associated with increased Fos expression in the LPAG [20]. Behavioral observations have shown that LPAG NMDA lesions interfere with prey hunting; the animals lost their motivation to pursue and attack prey without affecting general levels of arousal, locomotor activity, and regular feeding [22]. In line with these observations, the LPAG contains reward-excited neurons, which exhibited an increased firing rate in response to appetitive food [23]. Conversely, the LPAG has also been shown to respond to a conspecific aggressor. Thus, a significant Fos upregulation in the LPAG was found in animals exposed to dominant conspecifics [24]. In this regard, chemical and optogenetic stimulation experiments suggest that the LPAG mediates active defensive responses such as circa-strike defense, and that it supports a role in active social defensive behaviors to escape from a dominant's attacks [25 – 27].

Here, we investigated how the LPAG controls the opposite behavioral choices of predatory hunting and evasion from a social attack. We started by asking whether there is a differential activation of the neural populations in the LPAG activated during insect predation (IP) and social defeat (SD). To this end, we used an approach based on the temporal translational dynamics of the c-*fos* gene by combining immunofluorescence for Fos protein with fluorescent *in situ* hybridization for c-*fos* mRNA (Fos protein/c-*fos* mRNA IF-FISH) in animals exposed sequentially to IP and SD. We next examined the functional role of neural populations in the LPAG responsive to IP or SD by using pharmacogenetic silencing in Fos DD-Cre mice [28], which allowed targeting neural populations activated by a specific stimulus. Further, because the

lateral hypothalamic area (LHA) is one of the main targets of the LPAG [29], we used optogenetic inhibition and examined how LPAG projections to the LHA influence predatory and social defensive behaviors.

The LHA, in its turn, is involved in controlling predatory hunting and evasion from imminent threats [30]. In view of the fact that the LHA is heavily targeted by the LPAG, we also investigated how the LHA mediates IP and SD. First, we differentiated neuronal populations in the LHA responding to IP and SD using Fos protein/c-*fos* mRNA IF-FISH. Next, we determined the GABAergic and glutamatergic nature of LHA neurons responding to IP and SD using Fos protein/*VGAT* mRNA and Fos protein/*VGLUT2* mRNA IF-FISH. Finally, using VGAT-IRES-Cre and VGlut2-IRES-Cre mice, we applied pharmacogenetic tools to silence the activity of the LHA^{GABA} and LHA^{Glut} neurons selectively and then explored the functional role of LHA^{GABA} and LHA^{Glut} neurons on predatory hunting and social defensive behavior.

We here show that the LPAG contains two segregated neural populations that separately control opposite behavioral choices of predatory hunting and evasion from a social attack. Our findings are in line with the idea that the PAG works as a unique hub driving stereotyped responses and supplying primal emotional tone to influence complex aversive and appetitive responses [see 31]. Our results show that LPAG control over evasion in response to a social attack may be regarded as a stereotyped response depending most likely on descending projections to lower brainstem sites organizing the behavioral output. In contrast, the LPAG control over predatory behavior involves an ascending glutamatergic pathway to the LHA that likely influences LHA^{GABA} neurons to drive predatory hunting. This path putatively exerts a role in providing emotional drive for prey hunting and may conceivably have more widespread control on the motivational drive to seek other appetitive rewards.

Results

Identification of neuronal populations in LPAG activated by IP and SD

To differentiate neuronal populations in LPAG responding to insect predation (IP) and social defeat (SD), we combined immunofluorescence for Fos protein (IF) and fluorescent *in situ* hybridization for c-*fos* mRNA (FISH) following the protocol described by Marin-Blasco et al. [32]. Exposure to a first treatment increases c-*fos* mRNA levels, which reach a maximum level at about 20 min and decline to basal levels two hours later when the Fos protein is close to its maximum [33-35]. The animals are then exposed to a second stimulus, and a second peak of c-

fos mRNA will be observed about 20 min later. Thus, neurons responding to the first stimulus will show Fos protein (IF+/FISH-) mainly, neurons responding to the second stimulus will show mostly c-*fos* mRNA (IF-/FISH+), and those neurons activated by both stimuli will appear as double-labeled (IF+/FISH+). To determine the optimum exposure and sacrificing time points for our specific experimental conditions, we quantified the number of Fos protein- and c-*fos* mRNA positive-neurons in LPAG at different time points after IP and SD (see Figure S1**)**. As shown in Figure S1, two hours after the onset of IP, we found maximum levels of Fos protein levels and imperceptible c-*fos* mRNA signal; we obtained maximum c-*fos* mRNA levels 20 minutes after exposure to SD. However, low but perceptible newly synthesized Fos protein emerged at this time point in response to SD. Thus, we decided to shorten this time point to 15 minutes when c-*fos* mRNA levels are close to the maximum and less significant Fos protein levels were detected (Figure S1). Because exposure to a stressful stimulus such as SD affects motivation for hunting, we exposed animals first to IP and subsequently to SD. We also included two control groups of animals exposed twice to the same stimulus (groups IP+IP and SD+SD) to discard neuronal activation due to the mere manipulation of animals. Animals repeatedly exposed to the same stimulus showed reactivation of about 50% of neurons (IF+/FISH+ neurons) and a low number of IF-/FISH+ neurons (Figure 1A, C). Animals exposed sequentially to IP and SD showed reactivation of about 40% of neurons (IF+/FISH+). GzLM analysis of the number of newly activated neurons (IF–/FISH+) in animals exposed sequentially to IP and SD showed a significant effect of group factor (groups IP+IP, SD+SD, and IP+SD) [$\chi^2(2) = 165.57$, $p < 0.001$]. Pairwise comparisons indicate that the Group IP+SD presented a higher number of newly activated neurons (IF–/FISH+) when compared to IP+IP and SD+SD groups ($p < 0.001$) (Figure 1C).

It is important to note that the maximum levels of c-*fos* mRNA occur 20 minutes after the second stimulus (SD). However, we decided to sacrifice the animals 5 minutes earlier to minimize the detection of newly synthesized Fos protein. Thus, with this approach, the number of newly activated neurons (IF-/FISH+) could have been underestimated. Despite this caveat, the results suggest that exposure to SD induced activation of neurons already recruited by IP and also led to the recruitment of new neurons. Therefore, LPAG neuronal populations responding to predatory hunting and social defensive responses appear to be partially differentiated.

Functional analysis of neuronal populations in LPAG activated by IP and SD

In Fos DD-Cre mice, Cre recombinase is fused to an *E. coli* dihydrofolate reductase (ecDHFR)-derived destabilizing domain (DD-Cre) [36, 37] and is expressed under the control of the c-

fos promoter. The DD-Cre construct is unstable and degraded via proteasomes in the absence of the ecDHFR inhibitor trimethoprim (TMP). The intraperitoneal administration of TMP makes Cre recombinase stable (protected from degradation) and catalytically active (Figure 2A).

Here, Fos DD-Cre mice received bilateral injections in the LPAG of a Cre-dependent adeno-associated viral vector (AAV) expressing hM4D(Gi) inhibitory DREADD (Designer Receptor Exclusively Activated by Designer Drug) fused to an mCherry reporter (AAV5-hSyn-hM4D(Gi)-DIO-mCherry) to silence selectively the activity of LPAG neurons responsive to IP or SD (Figure 2A, B). Previous tract-tracing studies showed that LPAG neurons send substantial ascending projections to the LHA [22]. Therefore, we also aimed to detect possible differences in LHA projection patterns from LPAG-activated neurons in response to IP or SD. To this end, animals also received a paired injection of Cre-dependent AAV expressing an EYFP reporter (AAV5-hSyn-DIO-EYFP) for tracing ascending projections to the LHA (Figure 2B) and the descending projections to the brainstem (Figure S2). The EYFP reporter was used to trace LPAG projections because it yields a much stronger fluorescent signal than the reporter with mCherry fused to hM4D(Gi). The administration of TMP in animals previously exposed to IP or SD stabilizes DD-Cre expressed in active neurons and leads to Cre-dependent expression of hM4D(Gi) and EYFP (Figure 2A). Animals were subsequently treated with saline or clozepine-N-oxide (CNO) [38] and re-exposed to IP and SD for behavioral testing.

Previous studies showed that cytotoxic lesions in the LPAG increased the latency to start hunting and decreased the number of captured prey [22]. Therefore, during predatory hunting, we quantified the latency to catch the first cricket and the total number of crickets captured. Conversely, chemical and optogenetic stimulation experiments suggest that the LPAG mediates predominantly active defensive responses such as the circa-strike defense. This supports a role in active social defensive behaviors aimed at escaping from resident's attacks [25-27]. Thus, during the social agonistic interaction, we analyzed the number of intruder escapes in response to resident attacks (escape/attack ratio) as a measure of active defensive behavior.

CNO-induced inhibition of IP- and SD-responsive neurons on predatory behavior. For the latency to catch the first prey, univariate ANOVA revealed a significant interaction between the factors (time dependent Cre stabilization x treatment; $F_{1,21}=43,78$; $p<0.001$). Post hoc pairwise comparisons (Tukey's HSD test) revealed that IP Cre stabilized animals treated with CNO presented a significant increase in the latency to start hunting ($p<0.001$) (Figure 2D). IP Cre stabilized treated with CNO also presented a reduced number of captured crickets (Figure 2D).

In contrast, CNO-treated animals that received TMP Cre stabilization for SD did not differ from the saline-treated animals in the latency to start hunting (Tukey's HSD test, $p>0.26$) and the number of captured prey (Figure 2D).

CNO-induced inhibition of IP- and SD-responsive neurons on social defensive behavior. For the escape/attack ratio, univariate ANOVA revealed a significant interaction between the factors (time dependent Cre stabilization x treatment; $F1,21=30.8$; $p<0.001$). Post hoc pairwise comparisons (Tukey's HSD test) revealed that SD Cre stabilized animals treated with CNO presented a significant decrease in the escape/attack ratio observed during the social agonistic interaction ($p<0.001$) (Figure 2D). In contrast, CNO-treated animals that received TMP Cre stabilization for IP did not differ from the saline-treated animals in the escape/attack ratio observed during SD ($p>0.46$) (Figure 2D).

Thus, our functional analysis of Fos DD-Cre mice revealed that CNO inhibition of LPAG neurons activated in response to IP led to an increase in the latency to start hunting and a decrease in the total number of crickets captured but did not alter escape/attack ratio during SD. Conversely, CNO inhibition of LPAG SD-responding neurons did not change predatory behavior parameters and led to a decrease in the escape/attack ratio during SD.

The results of our pathway tracing analysis in Fos DD-Cre mice revealed that LPAG IP- and SD-responding neurons yielded a similar EYFP anterograde labeling in the LHA (Figure 2E) and brainstem (Figure S2).

Functional analysis of LHA-projecting LPAG terminals during IP and SD

The LPAG projects densely to the LHA, which is one of the main targets of the LPAG [22]. We next investigated whether the LPAG > LHA projection influences predatory and social defensive behaviors. Considering the predominantly excitatory nature of this projection (see Supplementary Material 3 and Figure S3), we employed a projection-based optogenetic silencing approach to examine the effect of inhibiting the LPAG > LHA projection on predatory hunting and social defense. For LPAG > LHA projection photoinhibition, we bilaterally injected the LPAG of C57BL/6 mice with adeno-associated viral (AAV) vectors encoding Archaerhodopsin 3 (eArch3)—a trafficking-enhanced light-sensitive (589 nm) proton pump [39] fused with enhanced yellow fluorescence protein (AAV5-hSyn-eArch3.0-EYFP) (Figure 3B). We included a control group of animals injected with a virus not expressing eArch3.0 (AAV-hSyn-EYFP-PA)

to discard light stimulation behavioral effects. The 561-nm laser light was continually delivered to the LHA during the 5 min of IP or SD through surgically implanted dual-fiber optic elements.

For the latency to catch the first prey, univariate ANOVA revealed a significant effect for the factor virus (eArch+ and control, $F_{1,8}=21.28$; $p<0.002$) and the factor treatment (laser on / off, $F_{1,8}=16.87$; $p<0.004$), and a significant interaction between the factors (virus x treatment, $F_{1,8}=32.21$; $p<0.001$). Post hoc pairwise comparisons (Tukey's HSD test) revealed that eArch+ animals during laser on presented a significant increase in the latency to catch the first prey (Figure 3D, $p<0.001$). Photoinhibition of the LPAG > LHA projection during IP also reduced the number of captured crickets (Figure 3C). For the escape/attack ratio, univariate ANOVA revealed no significant effect for the factors virus ($F_{1,8}=0.53$; $p=0.48$) and treatment ($F_{1,8}=0.21$; $p=0.659$) (Figure 3C).

Thus, our functional analysis revealed that photoinhibition of LPAG > LHA pathway impaired IP and increased the latency to start hunting while decreasing the total number of captured crickets; it did not alter escape/attack ratio during SD (Figure 3C).

Identification of neuronal populations in LHA activated by IP and SD

To differentiate neuronal populations in LHA responding to IP and SD, we next applied IF-FISH for Fos protein and c-*fos* mRNA [32]. Animals repeatedly exposed to the same stimulus (groups IP+IP and SD+SD) showed reactivation of about 40% of the neurons (IF+/FISH+ neurons) and an exceedingly low number of IF-/FISH+ neurons (Figure 4F, G). Animals exposed sequentially to IP and SD showed reactivation of about 38% of the neurons (IF+/FISH+) (Figure 4F, G). GzLM analysis of the number of newly activated neurons (IF–/FISH+) showed a significant effect of group factor (groups IP+IP, SD+SD, and IP+SD) [$\chi^2(2) = 36.17$, $p < 0.001$]. Pairwise comparisons indicate that the groups IP+IP and SD+SD did not differ in the number of newly activated neurons (IF–/FISH+), whereas the. group IP+SD presented a higher number of IF–/FISH+ neurons when compared to IP+IP and SD+SD groups ($p < 0.001$) (Figure 4F, G). Therefore, as it occurs in the LPAG, the LHA neuronal populations responding to predatory hunting and social defensive responses appear to be partially differentiated.

Characterization of GABAergic and glutamatergic LHA neurons responding to IP and SD

Recent optogenetic experiments suggest an essential role of LHA GABAergic neurons (LHA^{GABA}) in driving predatory hunting [30] as well as other motivated behaviors related to feeding [40-42]. Conversely, optogenetic stimulation of LHA glutamatergic neurons (LHA^{Glut})

induces a robust aversive response in the real-time place-preference assay [43]; LHA^{Glut} neurons increase their activity during evasion but not during food chasing [30]. To characterize the GABAergic and glutamatergic nature of the LHA neurons activated by IP and SD, we next combined immunofluorescence for Fos protein and fluorescent *in situ* hybridization for mRNAs of the vesicular transporters of GABA (*VGAT*) and glutamate (*VGLUT2*), respectively (Figure 4B, D).

GzLM analysis of the number of Fos/*VGAT* mRNA neurons showed a significant effect of group factor (groups Basal, IP, and SD) [$\chi^2(2) = 197.71$, $p < 0.001$]. Pairwise comparisons indicate that the SD group presented a lower number of Fos/*VGAT* mRNA neurons when compared to the IP group (*$p < 0.001$) (Figure 4C). Moreover, GzLM analysis of the number of Fos/*VGLUT2* mRNA neurons showed a significant effect of group factor [$\chi^2(2) = 86.75$, $p < 0.001$], and pairwise comparisons indicate that IP and SD groups did not differ in the number of Fos/*VGLUT2* mRNA neurons (Figure 4E).

The results suggest more significant recruitment of LHA^{GABA} neurons during predatory hunting, perhaps reflecting a more important role of LHA^{GABA} neurons in IP. Conversely, activation of LHA^{Glut} neurons was similar for both IP and SD. This does not infer a differential role of the LHA^{Glut} neurons in either of these behaviors.

Functional role of LHA^{GABA} and LHA^{Glut} neurons on predatory hunting and social defensive behavior

To address the behavioral role of LHA^{GABA} and LHA^{Glut} neurons in predatory hunting and social defensive responses, we used a Cre-dependent AAV vector expressing an inhibitory DREADD (AAV5-hSyn-H=hM4D(Gi)-DIO-mCherry in VGAT-IRES-Cre and VGlut2-IRES-Cre mice to silence the activity of the LHA^{GABA} and LHA^{Glut} neurons selectively (Figure 5A, B). We also included a group of control animals injected with a Cre-dependent AAV not expressing the inhibitory DREADD (AAV5-hSyn-DIO-EYFP).

CNO-induced inhibition of LHA^{GABA} neurons on predatory and social defensive behaviors in VGAT-IRES-Cre mice. For the latency to catch the first prey, univariate ANOVA revealed a significant effect for the factor virus (HM4D+ and control, $F_{1,12}= 9.04$; $p= 0.01$) and the factor treatment (CNO and Saline, $F_{1,12}= 124.46$; $p<0.001$), and a significant interaction between the factors (virus x treatment, $F_{1,12}= 39.9$; $p<0.001$). Post hoc pairwise comparisons (Tukey's HSD test) revealed that CNO treated HM4D+ animals presented a significant increase in the latency

to catch the first prey (*p<0.001) (Figure 5C). CNO treated HM4D+ animals also reduced the number of captured crickets (Figure 5C). For the escape/attack ratio during SD, univariate ANOVA revealed no significant effect for the factors virus ($F_{1,12}$= 0.61; p=0.45) and treatment ($F_{1,12}$=1.28; p=0.28) (Figure 5C).

CNO-induced inhibition of LHA^{Glut} neurons on predatory and social defensive behaviors in VGlut2-IRES-Cre mice. For the escape/attack ratio, univariate ANOVA revealed a significant effect for the factor virus (HM4D+ and control, $F_{1,8}$= 6.75; p= 0.032) and the factor treatment (CNO and Saline, $F_{1,8}$= 5.41; p= 0.048), and a significant interaction between the factors (virus x treatment, $F_{1,8}$= 14.12; p= 0.005). Post hoc pairwise comparisons (Tukey's HSD test) revealed that CNO treated HM4D+ animals presented a significant decrease in the escape/attack ratio (#p<0.01) (Figure 5D). For latency to start hunting, univariate ANOVA revealed no significant effect for the factors virus ($F_{1,8}$= 0.98; p= 0.35) and treatment ($F_{1,8}$= 0.04; p= 0.84). CNO treated HM4D+ animals also did not change the number of captured crickets (Figure 5D).

Our functional analysis revealed that pharmacogenetic inhibition of LHA^{GABA} neurons impaired IP by increasing the latency to start hunting and decreasing the total number of captured crickets, but it did not alter the escape/attack ratio during SD (Figure 5C). Conversely, pharmacogenetic inhibition of LHA^{Glut} neurons decreased the escape/attack ratio during SD but did not influence IP (Figure 5D).

Discussion

The experiments reported here address how the LPAG mediates the seemingly opposite behavioral choices of fleeing from a conspecific aggressor and prey hunting. First, we found that LPAG neuronal populations responding to predatory hunting and social defensive responses appear to be partially differentiated. Our functional analysis using Fos DD-Cre mice revealed that CNO-induced inhibition of LPAG neurons activated in response to IP disrupted prey hunting but did not alter escape/attack ratio during SD. Conversely, CNO-induced inhibition of LPAG SD-responding neurons did not change predatory behavior parameters and led to a decrease in the escape/attack ratio during SD. Thus, our functional analysis supports the idea of diverse neuronal populations in the LPAG influencing the predatory and social-defensive responses. In addition, we observed that photoinhibition of the LPAG > LHA pathway impaired IP but did not alter escape/attack ratio during SD. This suggests distinct axonal pathways from the LPAG play a role in organizing IP and SD.

To differentiate neuronal populations in LPAG responding to insect predation (IP) and social defeat (SD), we combined immunofluorescence for Fos protein (IF) and fluorescent *in situ* hybridization for c-*fos* mRNA (FISH) using sequential exposure to IP and SD. In response to the second stimulus (SD), we found a 35% increase in newly activated neurons. However, this measure of newly activated neurons may be an underestimate because we sacrificed the animals 5 minutes prior to the peak of c-*fos* mRNA levels to minimize the detection of newly synthesized Fos protein from the second stimulus. The activation of partially distinct LPAG neuronal populations in response to IP and SD may reflect the contribution of diverse sources of axonal inputs to the LPAG that are differentially activated during IP or SD. Thus, during IP, we have a striking activation of the lateral part of the superior colliculus' intermediate gray layer, which integrates critical sensory information to prey detection and projects to the LPAG [31, 44]. Conversely, animals exposed to a conspecific aggressor present strong activation in the ventrolateral part of the ventromedial hypothalamic nucleus and the dorsomedial pre-mammillary nucleus [24] that are relevant sources of inputs to the LPAG [24, 31].

Our functional analysis using pharmacogenetic inhibition in Fos DD-Cre mice revealed a clearer distinction between LPAG neural populations mediating IP and SD. Thus, CNO-induced inhibition of LPAG neurons activated in response to IP specifically impaired the IP behavioral parameters, but not the escape/attack ratio during SD. Conversely, the pharmacogenetic silencing of LPAG neurons activated in response to SD affected SD exclusively but not IP. Considering the large overlap between neuron populations activated during IP and SD, we would predict that the pharmacogenetic silencing would affect both responses regardless of the TMP time-dependent Cre stabilization for IP or SD. Thus, the results suggest that the non-overlapping LPAG neuronal population differentially activated in response to IP or SD should mediate the behavioral responses measured in this study. The present observations raise the interesting possibility that the LPAG neuronal population shared by IP and SD may conceivably mediate similar functional adjustments that occur during both responses whereas the other neuron population were activated explicitly during one type of behavior or the other to mediate the different behavioral outcomes.

The lateral hypothalamic area (LHA) is one of the main targets of LPAG projections [31], and we found that that LPAG IP- and SD-responding neurons yielded a similar EYFP anterograde labeling in LHA. LPAG contains mostly glutamatergic neurons [45]; in line with this data, we found that the vast majority of LPAG neurons activated during IP and SD co-expressed *VGLUT2*mRNA. Considering the predominantly excitatory nature of LPAG neurons

activated during IP and SD, we employed an optogenetic projection-based silencing approach to examine the effect of inhibiting the LPAG > LHA projection on predatory hunting and social defense. The results showed that photoinhibition of the LPAG > LHA pathway impaired IP but did not change SD.

The LHA is known to control predatory hunting, and the LPAG glutamatergic ascending projection to the LHA could provide motivational drive to LHA on predatory hunting. Our findings support the hypothesis that apart from organizing stereotyped responses, the PAG plays more complex roles by providing primal emotional tone to forebrain sites mediating complex behavioral responses [29]. In line with this view, an opioid-dependent mechanism in the LPAG has been shown to switch the motivation from maternal care to prey hunting in lactating rats [21, 46]. In addition, LPAG cytotoxic lesions impair place preference induced by morphine [47], thus suggesting an influence on the motivational drive to seek appetitive reward. Conversely, the ascending projection to the LHA from LPAG glutamatergic neurons does not seem to be critical for modulating SD. For this behavior, descending pathways from the LPAG to the brainstem are more likely to be involved in controlling escape responses during SD. In this regard, we have presently described the LPAG SD-responding neurons projections to several targets in the brainstem (see Figure S2).

The LHA has been implicated in controlling predatory hunting and threat evasion. LHA^{GABA} neurons promote feeding [30, 40-42] and predatory hunting including searching, pursuing, attacking, and capturing behaviors toward a moving prey [30]. Importantly, studies using pharmacogenetic manipulations showed that LHA^{GABA} neurons mediate consummatory behaviors regardless of the caloric content or biological relevance of the consumed stimuli [48]. Conversely, LHA^{GLUT} neurons may respond to aversive stimuli [43] and control evasion by predicting imminent dangers [30].

We found that LHA neuronal populations responding to predatory hunting and social defensive responses appear to be partially differentiated as observed by combining immunofluorescence for Fos protein and fluorescent *in situ* hybridization for c-*fos* mRNA in animals exposed sequentially to IP and SD. We next examined the GABAergic and glutamatergic nature of the LHA neurons activated during IP and SD. The results showed that the number of LHA^{GABA}-activated neurons was significantly higher after exposure to IP compared to SD whereas the number of LHA^{Glut}-activated neurons was comparable in both conditions. To address the behavioral role of LHA^{GABA} and LHA^{Glut} neurons on predatory hunting and social defensive

responses, we performed a pharmacogenetic inhibition in VGAT-IRES-Cre and VGlut2-IRES-Cre mice to silence the activity of LHA^{GABA} or LHA^{Glut} neurons selectively. Our functional analysis revealed that pharmacogenetic inhibition of LHA^{GABA} neurons impaired IP, increased the latency to start hunting, and decreased the total number of captured crickets; however, it did not alter evasion during SD. Conversely, pharmacogenetic inhibition of LHA^{Glut} neurons decreased the escape/attack ratio during SD but did not influence IP. Our results agree well with the literature and support the idea LHA^{GABA} neurons are involved in predatory hunting whereas the LHA^{Glut} neurons control evasion from aversive events. Li et al. [30] showed that LHA^{GABA} neurons drive predation through projections to the ventral tegmental area and ventrolateral PAG. Importantly, a GABAergic pathway from the central amygdalar nucleus to the ventrolateral PAG also drives predatory hunting [49]. Moreover, ventrolateral PAG local neurons might be responsible for the evasion behavior evoked by activation of LHA^{Glut} neurons [30]. Notably, as presently shown, ventrolateral PAG also receives a putative glutamatergic projection from the LPAG. In addition, the LHA^{Glut} neurons also promote aversive responses thorough a projection to the lateral habenula [43].

Our study showed that the LPAG contains two segregated neural populations that separately control opposite behavioral choices of predatory hunting and evasion from a social attack. The LPAG and the LHA appear to provide a parallel glutamatergic output to control evasion in response to a social attack. LPAG control over predatory behavior involves an ascending glutamatergic pathway to the LHA that likely influences LHA^{GABA} neurons driving predatory hunting. Studies examining morphine-related influences on maternal care and place preference suggest that, apart from prey hunting, this glutamatergic pathway from the LPAG to the LHA may exert more widespread control on the motivational drive to seek appetitive rewards. Future studies are needed to address the general role of the LPAG as a player in rewarding motivational mechanisms.

METHODS

Animals. Adult male mice, C57BL/6J, Fos DD-Cre, VGAT-ires-Cre and VGLUT-ires-Cre – all bred onto a C57BL/6J genetic background – were individually housed under controlled temperature (23º-25ºC) and 12h light cycle with free access to water and standard laboratory diet (Nuvilab-Quimtia, Brazil). At the time of the experiments, animals were 6-10 weeks old, weighting approximately 25-28 g. All experiments and conditions of animal housing were carried out under institutional guidelines [Colégio Brasileiro de Experimentação Animal (COBEA)] and

were in accordance with the NIH Guide for the Care and Use of Laboratory Animals (NIH Publications No. 80-23, 1996). Procedures were previously approved by the Committee on the Care and Use of Laboratory Animals of the Institute of Biomedical Sciences of the University of São Paulo, Brazil (Protocol number 085/2012). Experiments were always planned to minimize the number of animals used and their suffering.

C57BL/6J male mice (n = 90) were obtained from USP-local breeding facilities. Fos DD-Cre male mice (n = 14), were developed [see 28] and kindly provided by Dr Lisa Stowers Laboratory (Department of Neuroscience, The Scripps Research Institute, La Jolla, CA, USA). VGAT-ires-Cre (Slc32a1$^{tm2(cre)Lowl}$/J, n = 14) and VGLUT2-ires-Cre (Slc17a6$^{tm2(cre)Lowl}$/J, n = 10) knock-in male mice were acquired from Jackson Laboratories (stocks #016962 and #016963).

Viruses. For the functional analysis of neuronal populations in LPAG activated by IP and SD, Fos DD-Cre mice were injected bilaterally into the LPAG (Bregma AP –3.8, ML ±0.2, DV –2.4) with a mixture of 20 nl of AAV5-hSyn-hM4D(Gi)-DIO-mCherry (titer ≥ 5×10^{12} vg/mL) and 20 nl of AAV5-hSyn-DIO-EYFP (titer ≥ 7×10^{12} vg/mL) (Dr. Bryan Roth, University of North Carolina's Vector Core, NC, USA). For the functional analysis of LHA-projecting LPAG terminals, wild type mice were injected bilaterally into the LPAG with 40 nl of AAV5-hSyn-eArch3.0-EYFP (titer ≥ 4.4×10^{12} vg/mL) or AAV5-hSyn-EYFP-PA (titer ≥ 4.4×10^{12} vg/mL) (control virus) (Dr. Karl Deisseroth, University of North Carolina's Vector Core, NC, USA) and optical fibers were implanted bilaterally into LHA (Bregma AP –1.55, ML ±1.1, DV –4.9). For the functional analysis of LHA^{GABA} and LHA^{Glut} neurons on predatory hunting and social defensive behavior, VGLUT2-ires-Cre and VGAT-ires-Cre animals were injected bilaterally into LHA (Bregma AP –1.55, ML ±1.1, DV –5.1) with a mixture of 50 nl of AAV5-hSyn-hM4D(Gi)-DIO-mCherry and 50 nl of AAV5-hSyn-DIO-EYFP (control virus).

Stereotaxic surgery, viral injections and optical fiber implantation. Surgery for viral injection was performed at least 3 weeks before the first experimental day or the optical fiber implantation. During this time, animals remained undisturbed to recover from surgery and to allow viral expression. After the surgery for the implantation of optical fibers, animals remained undisturbed for one additional week to recover from surgery. For both viral injection and optic fiber implantation, mice were previously anesthetized in a box saturated with Isoforine (Cristália Laboratories, SP, Brazil) and then immediately head fixed on a stereotaxic instrument (Kopf Instruments, CA, USA). Anesthesia was maintained with 1-2% Isoforine/oxygen mix and body temperature was controlled with a heating pad. The scalp was incised and retracted, and the head

position was adjusted to place bregma and lambda in the same horizontal plane. Viral vectors were injected with a 5 µl Hamilton Syringe (Neuros Model 7000.5 KH). Injections were delivered at a rate of 10 nl/min using a motorized pump (Harvard Apparatus). The needle was left in place for 5 minutes after each injection to minimize upward flow of viral solution after raising the needle. Optical fibers (Mono Fiber-optic Cannulae 200/230-0.48, Doric Lenses Inc. Quebeq, Canada) were implanted and fixed onto animal skulls with dental resin (DuraLay, IL, USA). After the behavioral tests, animals were perfused to verify injection sites by visualization of fluorescent markers.

Behavioral procedures. *Predatory hunting paradigm.* The protocol used was adapted from Han et al. [49]. Adult crickets (*Gryllus assimilis*) were used as prey. One week before the first experimental day animals were habituated to cricket hunting by presenting three intact crickets for two consecutive days. Food restriction was not required. All animals captured and consumed all crickets during each habituation. During the behavioral tests, five intact crickets were presented. Animals were let to hunt during 5 minutes after the first predatory attack. Behavior was recorded for subsequent analysis of the latency to catch the first prey and the total number of crickets captured.

Resident-intruder paradigm. The protocol used was adapted from Miczek [50]. Adult Swiss male mice of approximately 14 weeks old, housed individually with sterilized but hormonally intact females, were used as residents. For the SD we used 8 residents, which were exposed only twice to intruders on the days of behavioral test. On the day of the behavioral test, the females were removed and replaced by intruders. The intruder was left interacting with the resident 5 minutes after the first attack. Behavior was recorded for subsequent analysis of the ratio of intruder escapes / resident attacks.

Experimental design. *Identification of neuronal populations in LPAG activated by IP and SD.* The aim of this experiment was to identify IP- and SD-responding neuronal populations in LPAG by Fos/c-*fos* mRNA IF-FISH double labeling. First, C57BL/6J mice (n = 47) were used to determine the c-*fos* mRNA and Fos protein temporal dynamics in response to IP and SD. To this end, animals were sacrificed at basal time (n = 3), 30 min (n = 4), 1 hour (n = 4), 2 hours (n = 4) and 4 hours (n = 4) after the onset of IP; and at basal time (n = 4), 10 min (n = 4), 20 min (n = 4), 30 min (n = 4), 1 hour (n = 4), 2 hours (n = 4) and 4 hours (n = 4) after the onset of SD. Next, C57BL/6J mice (n = 18) were distributed into 4 experimental groups: *BASAL GROUP* (n = 4), animals received no treatment; *IP+IP GROUP* (n = 4), animals were exposed to IP (5 minutes),

1 hour and 40 minutes later re-exposed to IP (5 minutes), and after the second IP, were left for 10 minutes undisturbed before perfusion; *SD+SD GROUP* (n = 4), animals were exposed to SD (5 minutes), 1 hour and 40 minutes later re-exposed to SD (5 minutes), and after the second SD, were left for 10 minutes undisturbed before perfusion; *IP+SD GROUP* (n = 6), animals were exposed to IP (5 minutes), 1 hour and 40 minutes later exposed to SD (5 minutes), and after the SD, were left for 10 minutes undisturbed before perfusion. Groups of animals exposed repeatedly to the same treatment (IP+IP and SD+SD) were included to discard neuronal activation due to the mere manipulation of animals. Immediately after the treatments, animals were anesthetized and perfused. Brains were extracted and processed for the simultaneous detection of Fos protein and c-*fos* mRNA by IF-FISH double labeling.

Characterization of GABA-ergic and glutamatergic phenotypic nature of IP- and SD-responding neurons in LPAG and LHA. C57BL/6J mice (n = 15) were distributed into 3 experimental groups: *BASAL GROUP* (n=3), animals received no treatment; *IP GROUP* (n=6), animals were exposed to IP (5 minutes) and left for 1 hour and 55 minutes undisturbed before perfusion; and *SD GROUP* (n = 6), animals were exposed to SD (5 minutes) and left for 1 hour and 55 minutes undisturbed before perfusion. Animals were anesthetized and perfused after the treatments. Brains were extracted and processed for Fos-*VGAT* mRNA and Fos-*VGLUT2* mRNA IF-FISH double labeling in LPAG and LHA.

Pharmacogenetic inhibition of IP- and SD-responding populations. Fos DD-Cre mice (n = 14) were distributed into 2 experimental groups: *IP-Cre stabilized GROUP* (n = 7), animals with Cre stabilization induced for predatory hunting; and *SD-Cre stabilized GROUP* (n = 7), animals with Cre stabilization induced for social defensive behavior. Animals were previously injected bilaterally into LPAG with AAV5-hSyn-hM4D(Gi)-DIO-mCherry and AAV5-hSyn-DIO-EYFP vectors. After 3 weeks, animals were exposed to IP (*IP-Cre stabilized GROUP)* or SD (*SD-Cre stabilized GROUP*). 10 minutes after exposure, TMP was administrated intraperitoneally (i.p.,170 mg/kg) for stabilization of Cre expressed in response to IP- or SD-active (Fos expressing) neurons. Animals were then kept undisturbed for 4 hours to allow stabilized Cre interacts with the viral vectors. After the procedure of Cre stabilization, animals remained undisturbed for 3 weeks to allow hM4D(Gi) expression before pharmacogenetic inhibition.

Optogenetic inhibition of LHA-projecting LPAG terminals. C57BL/6J mice (n = 10) were distributed into 2 experimental groups: *CONTROL GROUP* (n = 4), animals injected bilaterally into LPAG with an AAV vector not expressing eArch3.0 (AAV-hSyn-EYFP-PA); and *EARCH*

GROUP (n = 6), animals injected bilaterally into LPAG with an AAV vector expressing eArch3.0 (AAV5-hSyn-eArch3.0-EYFP). After 3 weeks, the animals received the optical fiber implantation, and remained undisturbed for 3 weeks before optogenetic inhibition.

Pharmacogenetic inhibition of LHA^{GABA} and LHA^{Glut} neurons. VGAT-ires-Cre mice (n = 14) were distributed into 2 experimental groups: *CONTROL GROUP* (n = 5), animals were injected bilaterally into LHA with a Cre-dependent AAV vector not expressing the inhibitory DREADD (AAV5-hSyn-DIO-EYFP); and *DREADD GROUP* (n = 9), animals were injected bilaterally into LHA with AAV5-hSyn-hM4D(Gi)-DIO-mCherry vector. VGLUT2-ires-Cre mice (n = 10) were distributed into 2 experimental groups: CONTROL GROUP (n = 5), animals were injected bilaterally into LHA with AAV5-hSyn-DIO-EYFP vector; and *DREADD GROUP* (n = 5), animals were injected bilaterally into LHA with AAV5-hSyn-hM4D(Gi)-DIO-mCherry vector. After surgery for viral injection, animals remained undisturbed for 3 weeks to allow viral expression before pharmacogenetic inhibition.

Pharmacogenetic inhibition. Animals were previously habituated to handling and injections for the 3 days before the first experimental day (one habituation session per day). After the handling session, animals received 250 µl of saline i.p. On the first experimental day (day 1), animals (IP-Cre stabilized and SD-Cre stabilized groups for Fos DD-Cre animals; and CONTROL and DREADD groups for VGAT-ires-Cre and VGLUT2-ires-Cre animals) were injected with saline i.p. and 30 minutes later they were tested for predatory behavior. On the next day (day 2), clozapine-N-Oxide (CNO; Tocris Bioscience, UK) was injected i.p (1 mg/kg) for the pharmacogenetic inhibition of IP- and SD-responding neurons in Fos DD-Cre mice, LHA^{GABA} in VGAT-ires-Cre mice, and LHA^{Glut} in VGLUT2-ires-Cre mice, and 30 minutes later, animals were tested again for predatory behavior. After three days (day 6), animals of all groups were injected with saline and 30 minutes later they were tested for social defensive behavior. On the next day (day 7), animals were injected with CNO and 30 minutes later, animals were tested again for social defensive behavior. Behavioral responses were recorded during all experimental sessions for subsequent analysis.

Optogenetic inhibition. For optogenetic inhibition, animals were previously habituated to the optogenetic cables for 3 consecutive days before the first experimental day (one habituation session per day). The habituation session consisted of plugging optogenetic cables to the implanted fiber-optic cannulae and letting the animals explore their home cage for 5 minutes without any additional stimulus. Optogenetic inhibition was induced by exposing animals

continuously to a yellow laser (589 nm, Low-Noise DPSS Laser System, Laserglow Techonologies). On experimental day 1, animals (groups CONTROL and EARCH) were exposed to predatory behavior with the yellow laser turned OFF. On experimental day 2, animals were exposed again to predatory behavior with the laser ON for the optogenetic inhibition of LHA terminals originating from LPAG. After three days (day 6), animals of both groups were exposed to social defensive behavior with the yellow laser turned OFF. On the next day (day 7), animals were animals were re-exposed to social defensive behavior with the laser ON. ON/OFF laser cycles were of 5 minutes for insect predation and 5 minutes for defensive behavior.

Perfusion and histological processing. After the experimental procedures, animals were anesthetized in a box saturated with Isoforine and fixed by transcardial perfusion, introducing first a physiological saline solution (0.4% NaCl) and then a fixative solution (4% PFA + 3.8% Borax). After perfusion, brains were removed, post-fixed in the same solution and embedded in a cryoprotectant solution containing 30% sucrose in potassium phosphate-buffered saline (KPBS; 0.2 M NaCl, 43 mM potassium phosphate). Brains were then frozen in dry ice cooled isopentane at -50 ºC, and preserved at -80 ºC. For cryosectioning, brains were embedded in O.C.T. compound (Fisher Healthcare, USA) and sectioned using a Leica CM1850 cryostat. 20 µm-thick transverse sections were collected in cryoprotectant solution (0.05M sodium phosphate buffer pH 7.3, 30% ethyleneglycol, 20% glycerol) and stored at -20 ºC.

IF-FISH double labeling. *Preparation and synthesis of RNA probes.* c-*fos* DIG antisense riboprobe was *in vitro* transcribed (DIG RNA Labeling Mix, Roche) from an EcoRI fragment of c-*fos* cDNA (Dr Inder Verma, The Salk Institute, CA, USA), subcloned into pBluescript SK-1 (Stratagene). This construction was generously provided by Dr Antonio Armario (Universidad Autónoma de Barcelona, Barcelona, Spain). VGAT and VGLUT2 DIG antisense riboprobes were transcribed *in vitro* from purified PCR-amplified DNA fragments (PureLink Quick Gel Extraction Kit, Invitrogen, CA, USA). Forward and reverse primers used were 5'-GCCATTCAGGGCATGTTC-3' and 5'-AGCAGCGTGAAGACCACC-3' for VGAT DIG antisense, and 5'-CCAAATCTTACGGTGCTACCTC-3' and 5'-TAGCCATCTTTCCTGTTCCACT-3' for VGLUT2 DIG riboprobe. After *in vitro* transcription, the product was heated during 5 minutes at 65 ºC. The probes were isolated through gel filtration columns (mini Quick Spin RNA Columns, Roche) and stored at -20ºC.

IF-FISH procedure. The protocol for IF-FISH was adapted from Marin-Blasco et al. [32]. All the solutions used were previously treated with diethylpyrocarbonate (DEPC) and sterilized to

ensure RNAse-free conditions. With the same purpose, glassware was previously baked at 200 ºC and all consumables were sterile or pretreated with RNase Away (Sigma). For the IF, free-floating sections were washed with KPBS to remove the cryoprotectant solution and then incubated directly with polyclonal rabbit anti-c-Fos (PC-38; Calbiochem-Millipore) at 1:20000 in 0.5% Blocking Reagent (Roche) in KPBS for 16 h at 4 ºC. Sections were then washed in KPBS and incubated with Anti-Rabbit Alexa 594 Goat IgG (H+L) (Invitrogen) at 1:500 during 2 h at random temperature (RT). Sections were then washed in KPBS and mounted on positive charged slides (Superfrost Plus, Thermo Scientific). FISH protocol was originally adapted from Simmons et al. [51]. Tissue was post-fixed in 4% PFA + 3.8% Borax, washed in KPBS and incubated for 15 minutes at 37 ºC in presence of proteinase K (Roche) at 0.01 mg⁄mL in an appropriate buffer (0.1M Tris–HCl pH 8.0, 50mM EDTA pH 8.0). Sections were then rinsed in DEPC-treated water and acetylated during 10 minutes in 0.25% acetic anhydrous in 0.1 M TEA (triethanolamine) pH 8.0. Finally, sections were washed in 2X concentrated saline-sodium citrate solution (SSC), dehydrated through graded concentrations of ethanol and air-dried. Thereafter, 100 µL of hybridization buffer (50% formamide, 0.3 M NaCl, 10 mM Tris-Cl pH 8.0, 1 mM EDTA pH 8.0, 1X Denhardts, 10% dextrane sulphate, yeast tRNA 500 µg⁄mL and 10 mM DTT) containing the DIG-labeled probe (1:2000) were added onto each slide and covered with a glass coverslip. Sections were incubated for 16-18 h in a humid chamber at 60 ºC. After this time, sections were washed in 4X SSC and RNA digested with RNase A (GE Healthcare) at 0.02 mg⁄mL in an appropriate buffer (0.5M NaCl, 10mM Tris–HCl pH 8.0, 1mM EDTA pH 8.0). After RNA digestion, sections were washed in descending concentrations of SSC (2X to 0.5X) containing 1mM DTT, and then heated at 60 ºC in 0.1X SSC during 30 min. Sections were then equilibrated in Tris-buffered saline with Tween 20 (T-TBS; 0.1 M Tris-HCl pH 7.5, 0.15 M NaCl, 0.05% Tween 20) and incubated for 30 minutes in blocking buffer [1% bovine serum albumin (BSA) in TBS]. Blocking buffer was then removed and a peroxidase-conjugated anti-DIG antibody (anti-DIG-POD, Roche) was added at 1:2000 in 1% BSA in T-TBS. After incubation during 2 hours at RT, slides were washed in T-TBS. Signal was amplified using a tyramide signal amplification kit (TSA-plus Fluorescein, PerkinElmer). After the amplification, nuclei were counterstained with DAPI (Sigma) at 1:20000 in TBS and mounted using an aqueous based mounting medium (Fluoromount, Sigma). Slides were stored at 4ºC in humid chambers until image capture.

Image capture and analysis. Brain regions of interest were determined using the Allen Brain Atlas. LPAG was captured and quantified at the level of the oculomotor nucleus (approximately between Bregma -3.79 mm and -4.23 mm). LHA was captured and quantified at the level of the

ventromedial nucleus (approximately between Bregma -1.43 mm and -1.80 mm). Images were captured using an epi-fluorescence microscope (NIKON, Eclipse E400) coupled to a digital camera (NIKON, DMX 1200). ImageJ public domain image processing software (FIJI v1.47f) was used for image analysis.

IF–FISH Double Labeling Images. Background signal was determined by the mean integrated density (ID) value of 10 unlabeled regions of interest (ROIs) per projection. IF and FISH particles were considered positive cells when ID value of ROIs exceeded 3 standard deviations over the average background. This resulted in 3 different types of cells: positive only for protein (IF+/FISH–), positive only for mRNA (IF–/FISH+), and double labeled (IF+/FISH+). Average of at least 6 fields (one field per hemisphere of three slices) per brain area / animal was used for the statistical analysis. Images were coded before counting. The number of positive particles was corrected by the quantified area and density was expressed as the number of cells per mm^2.

Behavioral analysis. All behavioral sessions were recorded using a high-speed (120fps) camera (DMC-FZ200, Panasonic) and they were blindly scored using an ethological analysis software "The Observer" (version 5.0; Noldus Information Technology, Wageningen, The Netherlands). For predatory behavior, the following behavioral items were encoded: 1) the latency to capture the first prey; and 2) the total number of crickets captured. For social defensive behavior, behavioral items were: 1) escape or flight: number of flight episodes of the intruder such as running away and jumping; and 2) attacks: chasing and biting of the intruder by the resident. The ratio between the number of escapes and attacks was processed as the frequency of the escapes for each attack episode.

Statistical analysis for cell counting. Statistical analysis was carried out with Statistical Package for Social Science software (SPSS, version 26 for Windows). Generalized linear model (GzLM) [52] was used to test between-subjects main effects. Significance is determined by the Wald chi-square statistic (χ^2). After the main analysis, appropriate pairwise comparisons were carried out and corrected by the Holm's Sequential Bonferroni Procedure [53]. The criterion for significance was set at $p<0.05$. Particular comparisons were planned to avoid or reduce corrections for multiple comparisons in all tests. All samples to be statistically compared were processed in the same assay to avoid inter-assay variability.

Statistical analysis for behavioral measurements. After testing for homogeneity of the variance with the Levene's test, our behavioral data (latency to start hunting and escape / attack ratio) were logarithmic transformed. The data were analyzed using 2 x 2 univariate ANOVAs for

each dependent variable (latency to start hunting and escape / attack ratio). The two factors (with two levels each) that entered the analysis were: time dependent Cre stabilization (during IP or SD) and treatment (CNO or saline) for the pharmacogenetic inhibition of neuronal populations in LPAG activated by IP and SD; virus (eArch+ and control) and treatment (laser on / off) for optogenetic inhibition of LHA-projecting LPAG terminals during IP and SD; and virus (hM4D+ and control) and treatment (CNO and saline) for the pharmacogenetic inhibition of GABAergic and glutamatergic LHA neurons during IP and SD. After obtaining a significant effect for each factor and a significant interaction between the factors, we applied Tukey's HSD test post hoc analysis to isolate the respective effects. For the total number of captured crickets observed during IP experiments, we used box plot graphical tool to represent the variation of the observed data. Two-tailed tests were used throughout the statistical analyses for both cell counting and behavioral measurements.

Figures

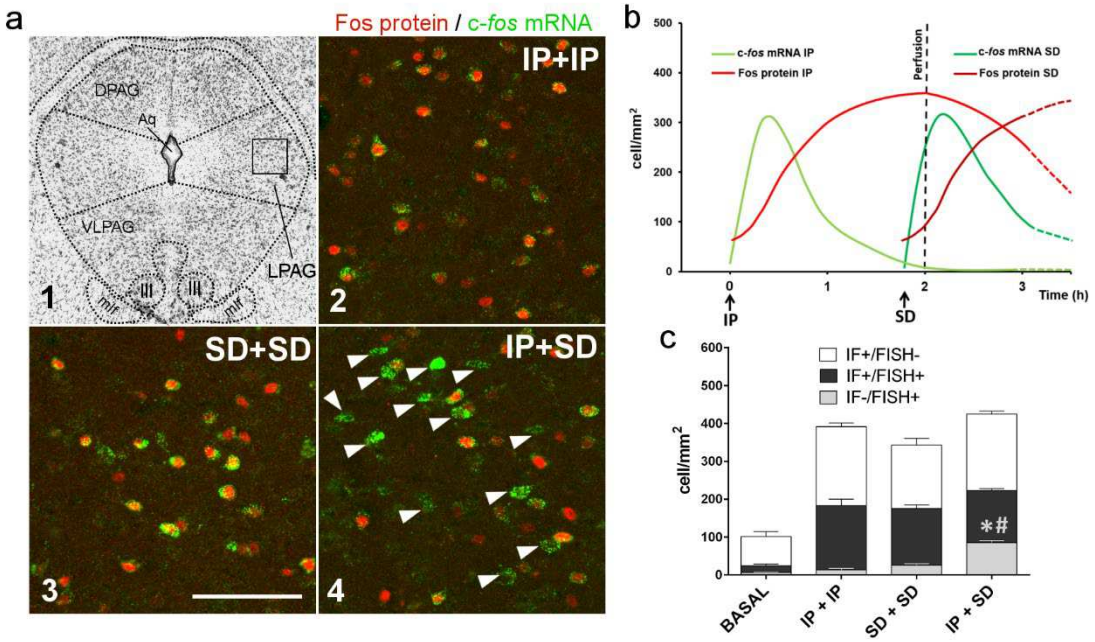

Figure 1. Identification of neuronal populations in LPAG activated by IP and SD.
a. a1. Photomicrograph of a representative transverse thionin-stained section of the LPAG at the level of the oculomotor nucleus (III). Square-delineated region indicates the approximate location of higher magnification fluorescence photomicrographs showing Fos protein/c-*fos* mRNA double labeling in (A2), (A3) and (A4). **a2-a4.** Representative Fos protein/c-*fos* mRNA double labeling fluorescence photomicrographs of groups IP+IP **(a2)**, SD+SD **(a3)**, and IP+SD **(a4)**. Fos protein positive cells are labeled in red (Alexa 594) and c-*fos* mRNA positive cells are labeled in green (FITC). Arrows indicate newly activated neurons (IF-/FISH+) in response to the second stimulus (SD). Abbreviations: Aq - central aqueduct; III - oculomotor nucleus; LPAG - periaquectudal gray, lateral part; mlf - medial longitudinal fascicle; VLPAG - periaquectudal gray, ventral lateral part. Scale bar, 100 µm.
b. Temporal dynamics of c-*fos* mRNA and Fos protein in response to IP and SD (see **Supplementary Fig. 1**). Note that the prefusion occurred 15 min after the set of SD, when c-*fos* mRNA levels are close to the maximum and no significant Fos protein levels in response to SD were detected.
c. Median values of the density of IF+/FISH-, IF-/FISH+, and IF+/FISH+ neurons across the groups. Group IP+SD presented a higher number of newly activated neurons (IF–/FISH+) when compared to IP+IP (*$p < 0.001$) and SD+SD (#$p < 0.001$). GzLM analysis followed with sequential Bonferroni corrections. Groups: BASAL (n = 4); IP+IP (n = 4); SD+SD (n = 4); IP+SD (n = 6). Data are reported as mean ± SEM.

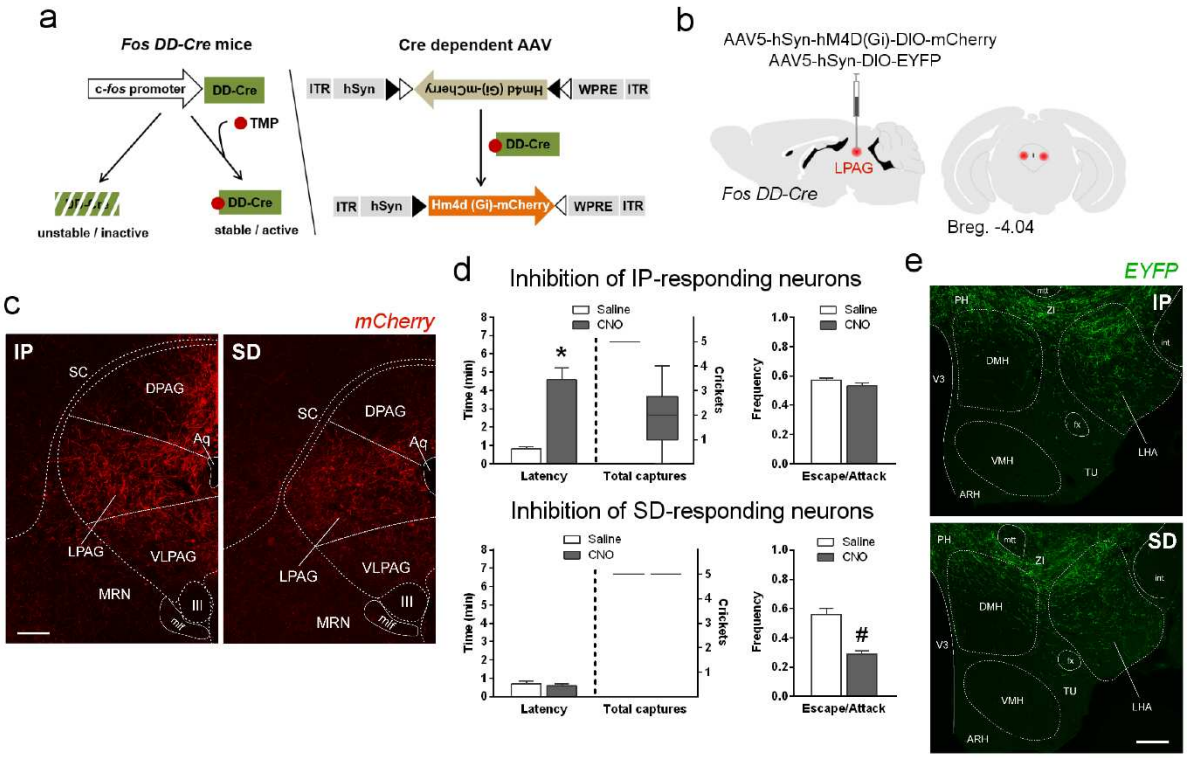

Figure 2. Pharmacogenetic inhibition of IP and SD-responding LPAG-neuronal populations.

a. Strategy for manipulation of active neurons in Fos DD-Cre mice. Administration of TMP induces stabilization of Cre recombinase expressed in active neurons thus promoting recombination in AAV vectors and expression of genes of interest – hM4D(Gi) inhibitory DREADD fused to mCherry and EYFP.

b. Schematics showing the location of the bilateral AAV viral vectors injection in the LPAG of Fos DD-Cre mice.

c. Fluorescence photomicrographs from representative cases showing mCherry expressing neurons activated in response to IP (left) and SD (right). Abbreviations: Aq - central aqueduct; DPAG - periaqueductal gray, dorsal part; III - oculomotor nucleus; LPAG - periaquectudal gray, lateral part; mlf - medial longitudinal fascicle; MRN - midbrain reticular nucleus; SC - superior colliculus; VLPAG - periaquectudal gray, ventral lateral part. Scale bar, 100 µm.

d. The effect of CNO-induced inhibition of IP- (top) and SD-responding (bottom) neurons on predatory (latency to catch the first prey and total number of captures; left) and social defensive (escape/attack ratio; right) behaviors. The data for latency and escape/attack ratio are shown as mean ± SEM, and the data for the number crickets captured are represented as box-whisker plots showing the median, interquartile range and minimum and maximum values. Groups: IP Cre stabilized animals (n = 7); SD Cre stabilized animals (n = 7). 2 x 2 univariate ANOVAs for each dependent variable (latency to start hunting and escape / attack ratio) followed by Tukey's HSD test post hoc analysis (*, $^{\#}p<0.001$).

e. Fluorescence photomicrographs from representative cases showing the distribution of projection to the LHA from LPAG EYFP expressing neurons activated during IP (top) and SD (bottom). Projections originating from IP- and SD-responding neurons yielded a similar EYFP anterograde labeling in LHA. Abbreviations: ARH - arcuate hypothalamus nucleus; DMH - dorsomedial nucleus of the hypothalamus; fx – fornix; int - internal capsule; LHA - lateral hypothalamic area; mtt - mammillothalamic tract; PH - posterior hypothalamic nucleus; TU - tuberal nucleus; V3 - third ventricle; ZI - zona incerta. Scale bar, 200 µm. **See S4 - videos**.

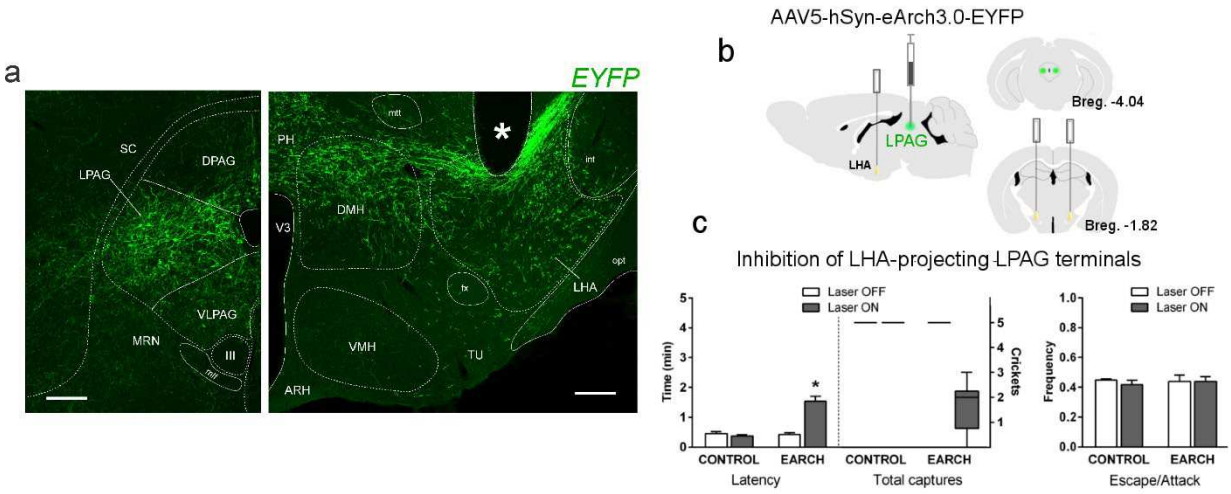

Figure 3. Optogenetic inhibition of LPAG-projecting LHA terminals in *C57BL/6 mice*.
a. Fluorescence photomicrographs illustrating the viral injection site in the LPAG with neurons expressing EYFP (left) and EYFP labeled fibers in LHA originating from LPAG (right). **(*)** tip of the optic fiber. Abbreviations: ARH - arcuate hypothalamus nucleus; DMH - dorsomedial nucleus of the hypothalamus; DPAG - periaqueductal gray, dorsal part; fx – fornix; III - oculomotor nucleus; int - internal capsule; LHA - lateral vestibular nucleus; LPAG - periaquectudal gray, lateral part; mlf - medial longitudinal fascicle; MRN - midbrain reticular nucleus; mtt - mammillothalamic tract; opt – optic tract; PH - posterior hypothalamic nucleus; SC - Superior colliculus; TU - tuberal nucleus; V3 - third ventricle; VLPAG - periaquectudal gray, ventral lateral part; VMH - ventralmedial nucleus of the hypothalamus Scale bars, 100 µm (PAG) and 200 µm (LHA).
b. Schematics showing the location of the bilateral AAV viral vectors injection in the LPAG and the position of bilateral optical fibers implanted in the LHA.
c. The effect of optogenetic inhibition of LPAG-projecting LHA terminals on predatory (latency to catch the first prey and total number of captures; left) and social defensive (escape/attack ratio; right) behaviors. The data for latency and escape/attack ratio are shown as mean ± SEM, and the data for the number crickets captured are represented as box-whisker plots showing the median, interquartile range and minimum and maximum values. Groups: CONTROL ($n = 4$) and EARCH ($n = 6$). 2 x 2 univariate ANOVAs for each dependent variable (latency to start hunting and escape / attack ratio) followed by Tukey's HSD test post hoc analysis (*$p<0.001$). **See S5-Videos.**

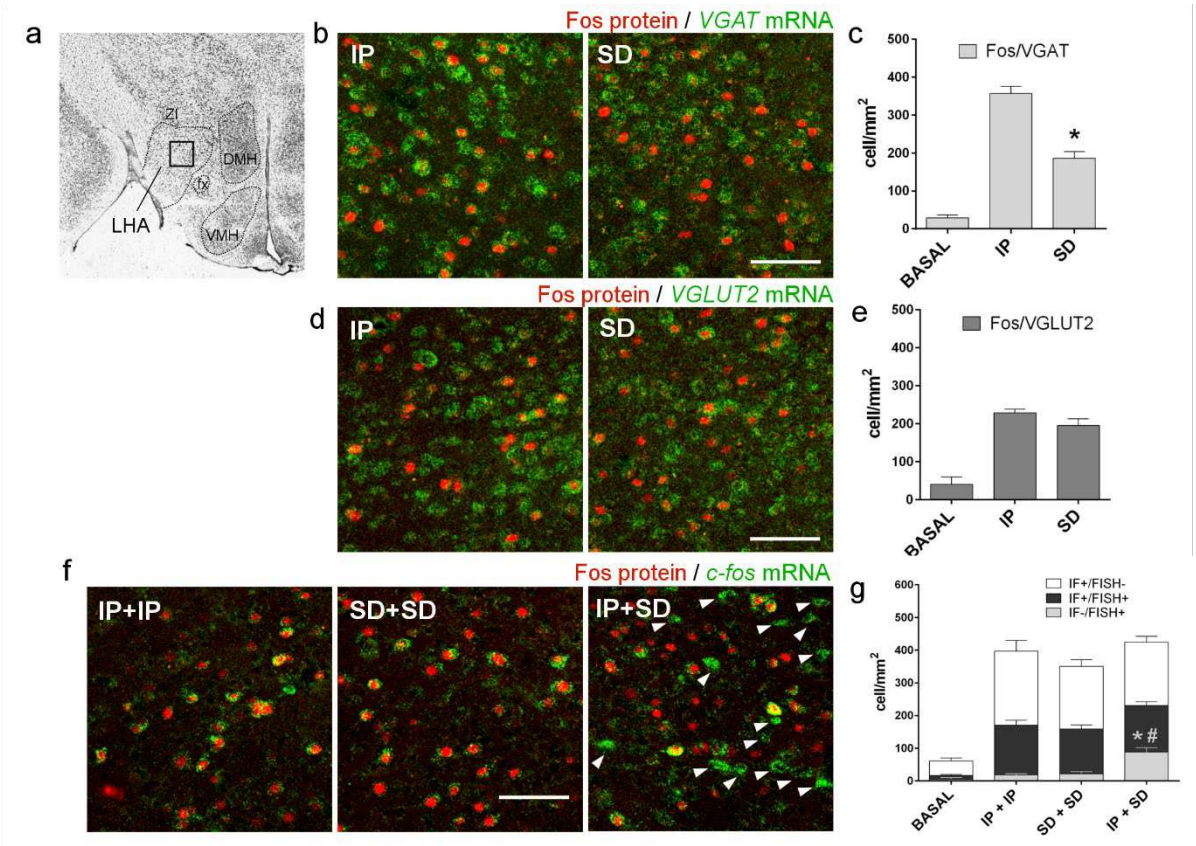

Figure 4. Analysis of the GABAergic and glutamatergic nature of LHA neurons recruited in response to predatory hunting and social defensive behavior and identification of LHA neural populations activated by IP and SD. a. Photomicrograph of a representative transverse thionin-stained section at tuberal levels of the LHA. Square-delineated region indicates the approximate location of higher magnification fluorescence photomicrographs showing Fos/VGAT and VGLUT2 mRNAs double labeling in (B) and (D). DMH – dorsomedial hypothalamic nucleus; fx – fornix; LHA – lateral hypothalamic area; ZI zona incerta. **b, d.** Representative fluorescence photomicrographs illustrating *Fos protein/VGAT* mRNA and *Fos protein/VGULT2* mRNA double labeling in the LHA of animals exposed to IP and SD. Fos protein positive cells are labeled in red (Alexa 594) and *VGAT* mRNA positive cells are labeled in green (FITC). Scale bar, 75 µm. **c, e.** Median values of the density of Fos protein/*VGAT*mRNA and *Fos protein/VGULT2* mRNA double labeled cells in the BASAL ($n = 3$), IP ($n = 6$), and SD ($n = 6$) groups. SD group presented a lower number of Fos/*VGAT* mRNA neurons when compared to IP group (*$p < 0.001$). IP and SD groups did not differ in the number of Fos protein/*VGLUT2* mRNA neurons. GzLM analysis followed with sequential Bonferroni corrections. Data are reported as mean ± SEM. **f.** Representative Fos protein/c-*fos* mRNA double labeling fluorescence photomicrographs of groups IP+IP, SD+SD, and IP+SD. Fos protein positive cells are labeled in red (Alexa 594) and c-*fos* mRNA positive cells are labeled in green (FITC). Arrows indicate newly activated neurons (IF-/FISH+) in response to the second stimulus (SD). Scale bar, 75 µm. **g.** Median values of the density of IF+/FISH-, IF-/FISH+, and IF+/FISH+ neurons in the BASAL ($n = 4$), IP+IP ($n = 4$), SD+SD ($n = 4$), and IP+SD ($n = 6$) groups. Group IP+SD presented a higher number of newly activated neurons (IF–/FISH+) when compared to IP+IP (*$p < 0.001$) and SD+SD (#$p < 0.001$). GzLM analysis followed with sequential Bonferroni corrections. Data are reported as mean ± SEM.

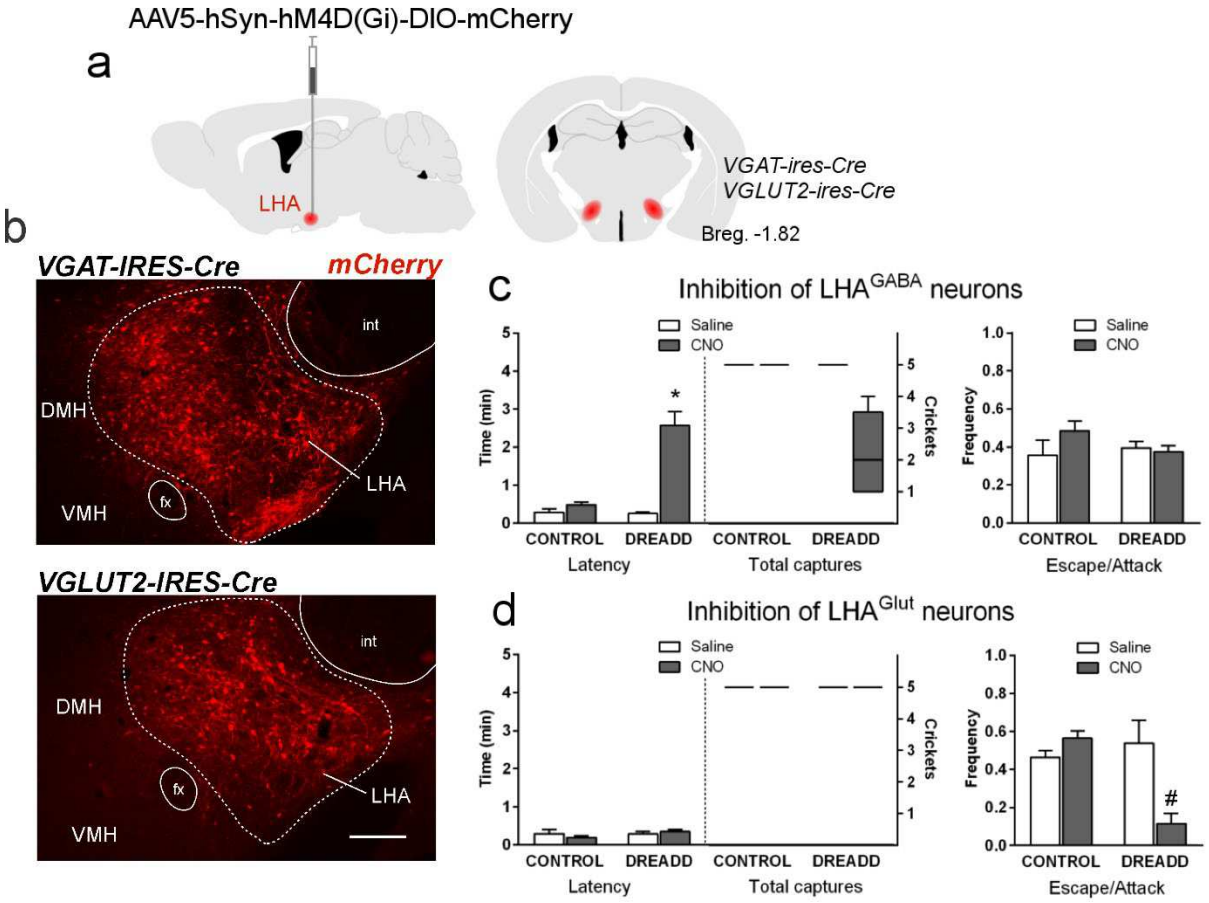

Figure 5. Functional role of LHA^{GABA} and LHA^{Glut} neurons on predatory hunting and social defensive behavior.

a. Schematics showing the bilateral injection in the LHA of Cre-dependent AAV expressing hM4D inhibitory DREADD in VGAT-IRES-Cre and VGLUT2-IRES-Cre mice.

b. Fluorescence photomicrographs showing neurons expressing mCherry (fused to HM4D) in the LHA of VGAT-IRES-Cre (top) and VGlut2-IRES-Cre (bottom) mice. DMH – dorsomedial hypothalamic nucleus; fx – fornix; int – internal capsule; LHA – lateral hypothalamic area; VMH – ventromedial hypothalamic nucleus. Scale bar, 200 µm.

c. The effect of CNO-induced inhibition of LHA^{GABA} neurons on predatory (latency to catch the first prey and total number of captures; left) and social defensive (escape/attack ratio; right) behaviors. The data for latency and escape/attack ratio are shown as mean ± SEM, and the data for the number crickets captured are represented as box-whisker plots showing the median, interquartile range and minimum and maximum values. Groups: CONTROL (n = 5); DREADD (n = 9). 2 x 2 univariate ANOVAs for each dependent variable (latency to start hunting and escape / attack ratio) followed by Tukey's HSD test post hoc analysis (*p<0.001).

d. The effect of CNO-induced inhibition of LHA^{Glut} neurons on predatory (latency to catch the first prey and total number of captures; left) and social defensive (escape/attack ratio; right) behaviors. The data for latency and escape/attack ratio are shown as mean ± SEM, and the data for the number crickets captured are represented as box-whisker plots showing the median, interquartile range and minimum and maximum values. Groups: CONTROL (n = 5); DREADD (n = 5). 2 x 2 univariate ANOVAs for each dependent variable (latency to start hunting and escape / attack ratio) followed by Tukey's HSD test post hoc analysis (#p<0.01). **See S6 – videos.**

Acknowledgments:

This research was supported by Fundação de Amparo à Pesquisa do Estado de São Paulo (FAPESP) Research Grants #2014/05432-9 (to NSC) and #2016/18667-0 (to SCM). FAPESP fellowships to IJMB (#2017/04830-9) and to MJRJ (#2017/09753-2). We thank Prof. Larry W. Swanson for insightful discussion and comments on the manuscript.

Author Contributions

IJMB, MJRJ, and NSC - conceptualized the project, designed the study, analyzed data, interpreted results prepared and edited the manuscript. SCM helped interpret the results and edit the manuscript. MVCB analyzed data and performed the statistical analysis. LS - contributed to the FosDDcre methodology and helped edit the manuscript. IJMB and MJRJ performed experiments.

Financial Disclosures/Conflict of Interest

The authors have no competing financial interests or potential conflicts of interest.

References

1. Sakuma, Y. & Pfaff, D. W. Facilitation of female reproductive behavior from mesencephalic central gray in the rat. *Am. J. Physiol.* - Regul. Integr. Comp. Physiol. **6**, (1979).

2. Besson, J.-M., Fardin, V. & Olivéras, J.-L. Analgesia Produced by Stimulation of the Periaqueductal Gray Matter: True Antinoceptive Effects Versus Stress Effects. in The Midbrain Periaqueductal Gray Matter 121–138. *Springer US* (1991).

3. Fanselow, M. S. The Midbrain Periaqueductal Gray as a Coordinator of Action in Response to Fear and Anxiety. in The Midbrain Periaqueductal Gray Matter 151–173. *Springer US* (1991).

4. Lovick, T. A. Integrated activity of cardiovascular and pain regulatory systems: Role in adaptive behavioural responses. *Progr.Neurobiol.* **40**, 631–644 (1993).

5. Bandler, R. & Shipley, M. T. Columnar organization in the midbrain periaqueductal gray: modules for emotional expression? *Trends Neurosci.* **17**, 379–89 (1994).

6. Jürgens, U. The role of the periaqueductal grey in vocal behaviour. *Behav. Brain Res*. **62** 107–117 (1994).

7. Lonstein, J. S. & Stern, J. M. Role of the midbrain periaqueductal gray in maternal nurturance and aggression: C-fos and electrolytic lesion studies in lactating rats. *J. Neurosci.* **17**, 3364–3378 (1997).

8. Lonstein, J. S. & Stern, J. M. Site and behavioral specificity of periaqueductal gray lesions on postpartum sexual, maternal, and aggressive behaviors in rats. *Brain Res.* **804**, 21–35 (1998).

9. Gruber-Dujardin, E. Role of the periaqueductal gray in expressing vocalization. in *Handbook of Behavioral Neuroscience* vol. **19**, 313–327 (2010).

10. Cezario, A. F., Ribeiro-Barbosa, E. R., Baldo, M. V. C. & Canteras, N. S. Hypothalamic sites responding to predator threats - The role of the dorsal premammillary nucleus in unconditioned and conditioned antipredatory defensive behavior. *Eur. J. Neurosci.* **28**, 1003–1015 (2008).

11. Sukikara, M. H., Mota-Ortiz, S. R., Baldo, M. V., Felicio, L. F. & Canteras, N. S. The periaqueductal gray and its potential role in maternal behavior inhibition in response to predatory threats. *Behav. Brain Res.* **209**, 226–233 (2010).

12. Pobbe, R. L. H., Zangrossi, H., Blanchard, D. C. & Blanchard, R. J. Involvement of dorsal raphe nucleus and dorsal periaqueductal gray 5-HT receptors in the modulation of mouse defensive behaviors. *Eur. Neuropsychopharmacol.* **21**, 306–315 (2011)

13. Souza, R. R. & Carobrez, A. P. Acquisition and expression of fear memories are distinctly modulated along the dorsolateral periaqueductal gray axis of rats exposed to predator odor. *Behav. Brain Res.* **315**, 160–167 (2016).

14. Di Scala, G., Mana, M. J., Jacobs, W. J. & Phillips, A. G. Evidence of Pavlovian conditioned fear following electrical stimulation of the periaqueductal grey in the rat. *Physiol. Behav.* **40**, 55–63 (1987).

15. Di Scala, G. & Sandner, G. Conditioned place aversion produced by microinjections of semicarbazide into the periaqueductal gray of the rat. *Brain Res.* **483**, 91–97 (1989).

16. Kincheski, G. C., Mota-Ortiz, S. R., Pavesi, E., Canteras, N. S. & Carobrez, A. P. The Dorsolateral Periaqueductal Gray and Its Role in Mediating Fear Learning to Life Threatening Events. *PLoS One* 7, e50361 (2012).

17. Kim, E. J. et al. Dorsal periaqueductal gray-amygdala pathway conveys both innate and learned fear responses in rats. *Proc. Natl. Acad. Sci.* U. S. A. **110**, 14795–14800 (2013).

18. Deng, H., Xiao, X. & Wang, Z. Periaqueductal gray neuronal activities underlie different aspects of defensive behaviors. *J. Neurosci.* **36**, 7580–7588 (2016).

19. de Andrade Rufino, R., Mota-Ortiz, S. R., De Lima, M. A. X., Baldo, M. V. C. & Canteras, N. S. The rostrodorsal periaqueductal gray influences both innate fear responses and acquisition of fear memory in animals exposed to a live predator. *Brain Struct. Funct.* **224**, 1537–1551 (2019).

20. Comoli, E., Ribeiro-Barbosa, E. R. & Canteras, N. S. Predatory hunting and exposure to a live predator induce opposite patterns of Fos immunoreactivity in the PAG. *Behav. Brain Res.* **138**, 17–28 (2003).

21. Sukikara, M. H., Mota-Ortiz, S. R., Baldo, M. V., Felício, L. F. & Canteras, N. S. A role for the periaqueductal gray in switching adaptive behavioral responses. *J. Neurosci.* **26**, 2583–2589 (2006).

22. Mota-Ortiz, S. R. et al. The periaqueductal gray as a critical site to mediate reward seeking during predatory hunting. *Behav. Brain Res.* **226**, 32–40 (2012).

23. Tryon, V. L. & Mizumori, S. J. Y. A novel role for the periaqueductal gray in consummatory behavior. *Front. Behav. Neurosci.* **12**, (2018).

24. Motta, S. C. et al. Dissecting the brain's fear system reveals the hypothalamus is critical for responding in subordinate conspecific intruders. *Proc. Natl. Acad. Sci. U. S. A.* **106**, 4870–4875 (2009).

25. Depaulis, A., Keay, K. A. & Bandler, R. Longitudinal neuronal organization of defensive reactions in the midbrain periaqueductal gray region of the rat. *Exp. Brain Res.* **90**, 307–318 (1992).

26. Assareh, N., Sarrami, M., Carrive, P. & McNally, G. P. The organization of defensive behavior elicited by optogenetic excitation of rat lateral or ventrolateral periaqueductal gray. *Behav. Neurosci.* **130**, 406–414 (2016).

27. Wang, L. et al. Hypothalamic Control of Conspecific Self-Defense. *Cell Rep.* **26**, 1747-1758.e5 (2019).

28. Dillingham, B. C. et al. Fear Learning Induces Long-Lasting Changes in Gene Expression and Pathway Specific Presynaptic Growth. *bioRxiv* 571331 (2019)

29. Motta, S. C., Carobrez, A. P. & Canteras, N. S. The periaqueductal gray and primal emotional processing critical to influence complex defensive responses, fear learning and reward seeking. *Neurosci. Biobehav. Rev.* **76**, 39–47 (2017).

30. Li, Y. et al. Hypothalamic Circuits for Predation and Evasion. *Neuron* **97**, 911-924.e5 (2018).

31. Mota-Ortiz, S. R., Sukikara, M. H., Felicio, L. F. & Canteras, N. S. Afferent connections to the rostrolateral part of the periaqueductal gray: A critical region influencing the motivation drive to hunt and forage. *Neural Plast.* (2009).

32. Marín-Blasco, I., Muñoz-Abellán, C., Andero, R., Nadal, R. & Armario, A. Neuronal Activation After Prolonged Immobilization: Do the Same or Different Neurons Respond to a Novel Stressor? *Cereb. Cortex* **28**, 1233–1244 (2018).

33. Kovács, K. J. & Sawchenko, P. E. Sequence of stress-induced alterations in indices of synaptic and transcriptional activation in parvocellular neurosecretory neurons. *J. Neurosci.* **16**, 262–273 (1996).

34. Zangenehpour, S. & Chaudhuri, A. Differential induction and decay curves of c-*fos* and *zif268* revealed through dual activity maps. *Mol. Brain Res.* **109**, 221–225 (2002).

35. Kovács, K. J. Measurement of immediate-early gene activation- c-fos and beyond. J. *Neuroendocrinol.* **20**, 665–672 (2008).

36. Iwamoto, M., Björklund, T., Lundberg, C., Kirik, D. & Wandless, T. J. A general chemical method to regulate protein stability in the mammalian central nervous system. *Chem. Biol*. **17**, 981–988 (2010).

37. Sando, R. et al. Inducible control of gene expression with destabilized Cre. *Nat. Methods* **10**, 1085–1088 (2013).

38. Armbruster, B. N., Li, X., Pausch, M. H., Herlitze, S. & Roth, B. L. Evolving the lock to fit the key to create a family of G protein-coupled receptors potently activated by an inert ligand. *Proc. Natl. Acad. Sci. U. S. A.* **104**, 5163–5168 (2007).

39. Mattis, J. et al. Principles for applying optogenetic tools derived from direct comparative analysis of microbial opsins. *Nat. Methods* **9**, 159–172 (2012).

40. Jennings, J. H., Rizzi, G., Stamatakis, A. M., Ung, R. L. & Stuber, G. D. The Inhibitory Circuit Architecture of the Lateral Hypothalamus Orchestrates Feeding. *Science* (80) **341**, 1517–1521 (2013).

41. Jennings, J. H. et al. Visualizing hypothalamic network dynamics for appetitive and consummatory behaviors. *Cell* **160**, 516–527 (2015).

42. O'Connor, E. C. et al. Accumbal D1R Neurons Projecting to Lateral Hypothalamus Authorize Feeding. *Neuron* **88**, 553–564 (2015).

43. Lazaridis, I. et al. A hypothalamus-habenula circuit controls aversion. *Mol. Psychiatry* **24**, 1351–1368 (2019).

44. Furigo, I. C. et al. The role of the superior colliculus in predatory hunting. *Neuroscience* **165**, 1–15 (2010).

45. Lein, E. S. et al. Genome-wide atlas of gene expression in the adult mouse brain. *Nature* **445**, 168–176 (2007).

46. Miranda-Paiva, C. M., Ribeiro-Barbosa, E. R., Canteras, N. S. & Felicio, L. F. A role for the periaqueductal grey in opioidergic inhibition of maternal behaviour. *Eur. J. Neurosci.* **18**, 667–674 (2003).

47. De Oliveira, W.F. Analysis of the rostrolateral portion of the periaqueductal gray (PAGrl) in drug seeking behavior. Ph.D. Thesis. Institute of Biomedical Sciences. University of São Paulo. pp. 86 (2015).

48. Navarro, M. et al. Lateral hypothalamus GABAergic neurons modulate consummatory behaviors regardless of the caloric content or biological relevance of the consumed stimuli. *Neuropsychopharmacology* **41**, 1505–1512 (2016).

49. Han, W. et al. Integrated Control of Predatory Hunting by the Central Nucleus of the Amygdala. *Cell* **168**, 311-324.e18 (2017).

50. Miczek, K. A. A new test for aggression in rats without aversive stimulation: Differential effects of d-amphetamine and cocaine. *Psychopharmacology* (Berl). **60**, 253–259 (1979).

51. Simmons, D. M., Arriza, J. L. & Swanson, L. W. A complete protocol for in situ hybridization of messenger RNAs in brain and other tissues with radiolabeled single-stranded RNA probes. *J. Histotechnol.* **12**, 169–181 (1989).

52. McCulloch C. E., Searle S.R. Generalized, linear, and mixed models. *New York: John Wiley & Sons* (2001).

53. Holm, S. A simple sequentially rejective multiple test procedure. *Scand. J. Stat*. **6**, 65–70 (1979).

Figures

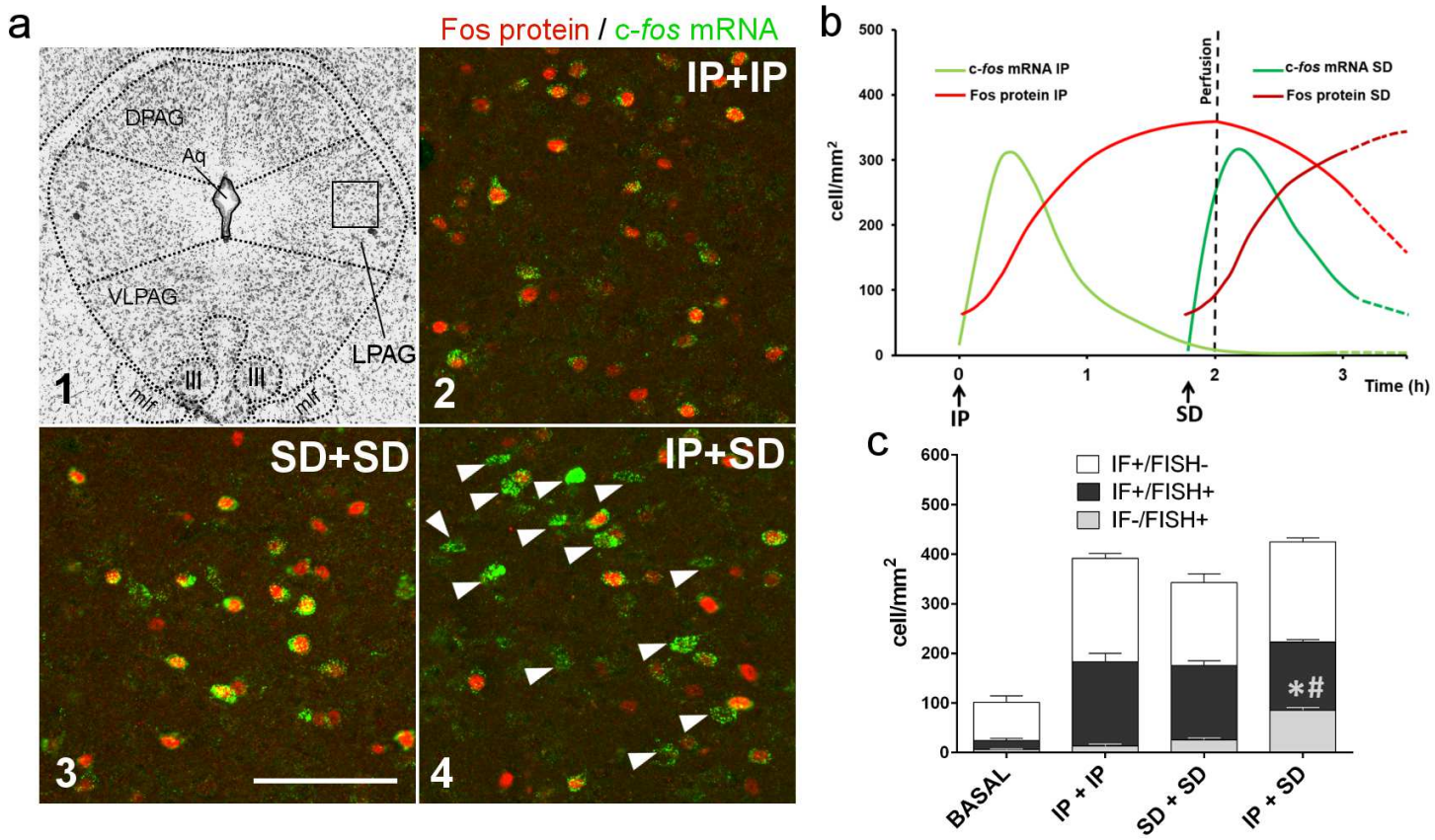

Figure 1

Identification of neuronal populations in LPAG activated by IP and SD. a. a1. Photomicrograph of a representative transverse thionin-stained section of the LPAG at the level of the oculomotor nucleus (III). Square-delineated region indicates the approximate location of higher magnification fluorescence photomicrographs showing Fos protein/c-fos mRNA double labeling in (A2), (A3) and (A4). a2-a4. Representative Fos protein/c-fos mRNA double labeling fluorescence photomicrographs of groups IP+IP (a2), SD+SD (a3), and IP+SD (a4). Fos protein positive cells are labeled in red (Alexa 594) and c-fos mRNA positive cells are labeled in green (FITC). Arrows indicate newly activated neurons (IF-/FISH+) in response to the second stimulus (SD). Abbreviations: Aq - central aqueduct; III - oculomotor nucleus; LPAG - periaquectudal gray, lateral part; mlf - medial longitudinal fascicle; VLPAG - periaquectudal gray, ventral lateral part. Scale bar, 100 µm. b. Temporal dynamics of c-fos mRNA and Fos protein in response to IP and SD (see Supplementary Fig. 1). Note that the prefusion occurred 15 min after the set of SD, when c-fos mRNA levels are close to the maximum and no significant Fos protein levels in response to SD were detected. c. Median values of the density of IF+/FISH-, IF-/FISH+, and IF+/FISH+ neurons across the groups. Group IP+SD presented a higher number of newly activated neurons (IF−/FISH+) when compared to IP+IP (*$p < 0.001$) and SD+SD (#$p < 0.001$). GzLM analysis followed with sequential Bonferroni corrections. Groups: BASAL (n = 4); IP+IP (n = 4); SD+SD (n = 4); IP+SD (n = 6). Data are reported as mean ± SEM.

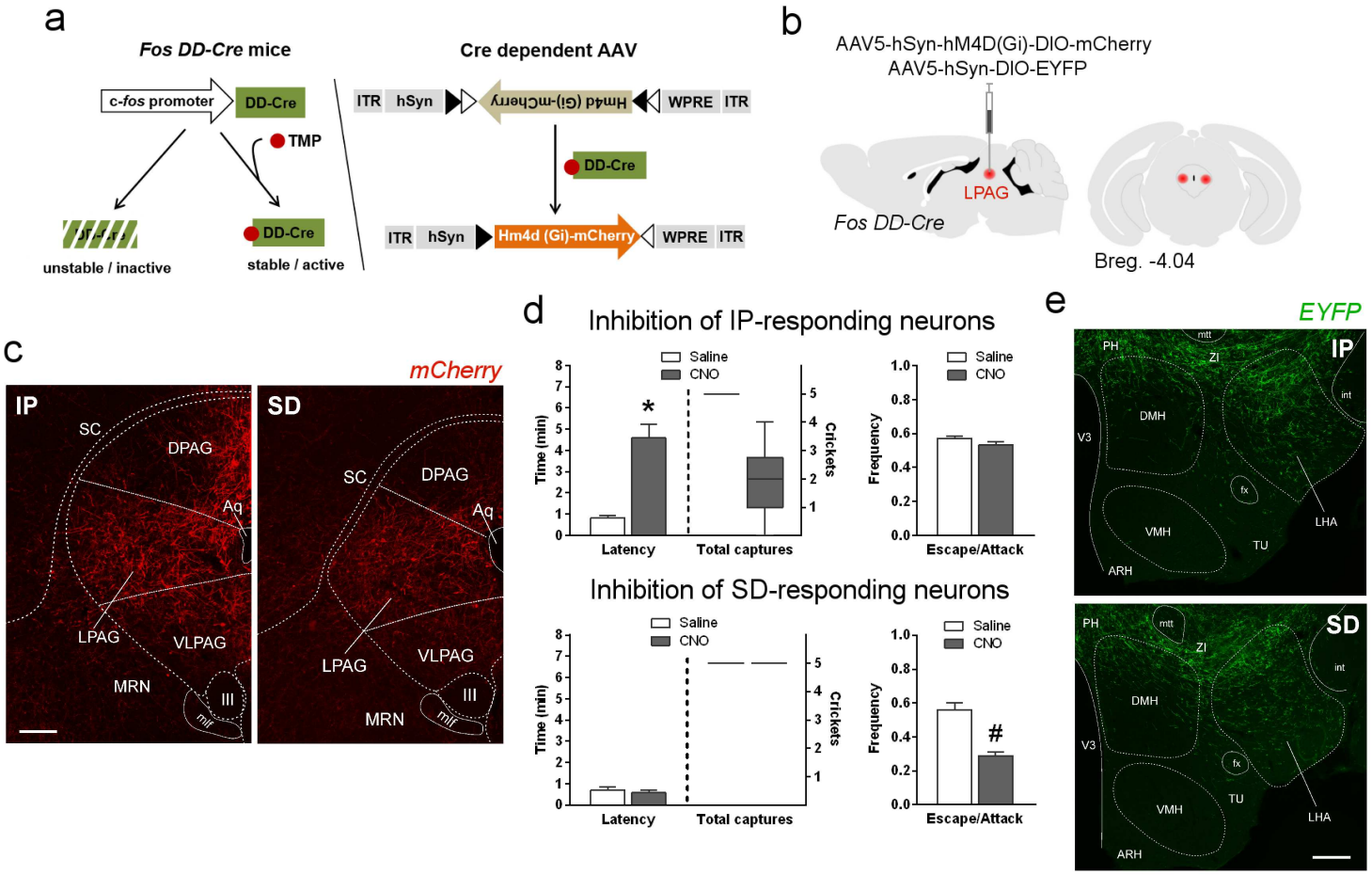

Figure 2

Pharmacogenetic inhibition of IP and SD-responding LPAG-neuronal populations. a. Strategy for manipulation of active neurons in Fos DD-Cre mice. Administration of TMP induces stabilization of Cre recombinase expressed in active neurons thus promoting recombination in AAV vectors and expression of genes of interest – hM4D(Gi) inhibitory DREADD fused to mCherry and EYFP. b. Schematics showing the location of the bilateral AAV viral vectors injection in the LPAG of Fos DD-Cre mice. c. Fluorescence photomicrographs from representative cases showing mCherry expressing neurons activated in response to IP (left) and SD (right). Abbreviations: Aq - central aqueduct; DPAG - periaqueductal gray, dorsal part; III - oculomotor nucleus; LPAG - periaquectudal gray, lateral part; mlf - medial longitudinal fascicle; MRN - midbrain reticular nucleus; SC - superior colliculus; VLPAG - periaquectudal gray, ventral lateral part. Scale bar, 100 µm. d. The effect of CNO-induced inhibition of IP- (top) and SD-responding (bottom) neurons on predatory (latency to catch the first prey and total number of captures; left) and social defensive (escape/attack ratio; right) behaviors. The data for latency and escape/attack ratio are shown as mean ± SEM, and the data for the number crickets captured are represented as box-whisker plots showing the median, interquartile range and minimum and maximum values. Groups: IP Cre stabilized animals (n = 7); SD Cre stabilized animals (n = 7). 2 x 2 univariate ANOVAs for each dependent variable (latency to start hunting and escape / attack ratio) followed by Tukey's HSD test post hoc analysis (*, #p<0.001). e. Fluorescence photomicrographs from representative cases showing the distribution of projection to the

LHA from LPAG EYFP expressing neurons activated during IP (top) and SD (bottom). Projections originating from IP- and SD-responding neurons yielded a similar EYFP anterograde labeling in LHA. Abbreviations: ARH - arcuate hypothalamus nucleus; DMH - dorsomedial nucleus of the hypothalamus; fx – fornix; int - internal capsule; LHA - lateral hypothalamic area; mtt - mammillothalamic tract; PH - posterior hypothalamic nucleus; TU - tuberal nucleus; V3 - third ventricle; ZI - zona incerta. Scale bar, 200 µm. See S4 - videos.

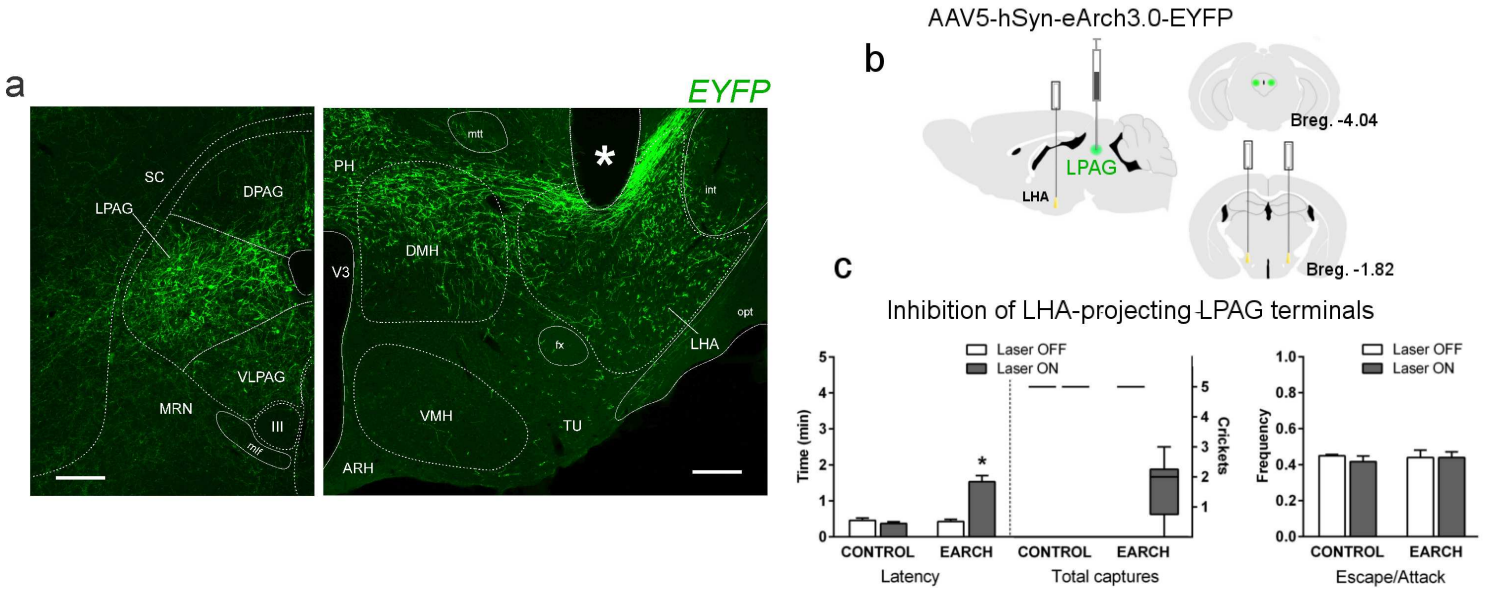

Figure 3

Optogenetic inhibition of LPAG-projecting LHA terminals in C57BL/6 mice. a. Fluorescence photomicrographs illustrating the viral injection site in the LPAG with neurons expressing EYFP (left) and EYFP labeled fibers in LHA originating from LPAG (right). (*) tip of the optic fiber. Abbreviations: ARH - arcuate hypothalamus nucleus; DMH - dorsomedial nucleus of the hypothalamus; DPAG - periaqueductal gray, dorsal part; fx – fornix; III - oculomotor nucleus; int - internal capsule; LHA - lateral vestibular nucleus; LPAG - periaquectudal gray, lateral part; mlf - medial longitudinal fascicle; MRN - midbrain reticular nucleus; mtt - mammillothalamic tract; opt – optic tract; PH - posterior hypothalamic nucleus; SC - Superior colliculus; TU - tuberal nucleus; V3 - third ventricle; VLPAG - periaquectudal gray, ventral lateral part; VMH - ventralmedial nucleus of the hypothalamus Scale bars, 100 µm (PAG) and 200 µm (LHA). b. Schematics showing the location of the bilateral AAV viral vectors injection in the LPAG and the position of bilateral optical fibers implanted in the LHA. c. The effect of optogenetic inhibition of LPAG-projecting LHA terminals on predatory (latency to catch the first prey and total number of captures; left) and social defensive (escape/attack ratio; right) behaviors. The data for latency and escape/attack ratio are shown as mean ± SEM, and the data for the number crickets captured are represented as box-whisker plots showing the median, interquartile range and minimum and maximum values. Groups: CONTROL (n = 4) and EARCH (n = 6). 2 x 2 univariate ANOVAs for each dependent variable (latency to start hunting and escape / attack ratio) followed by Tukey's HSD test post hoc analysis (*p<0.001). See S5- Videos.

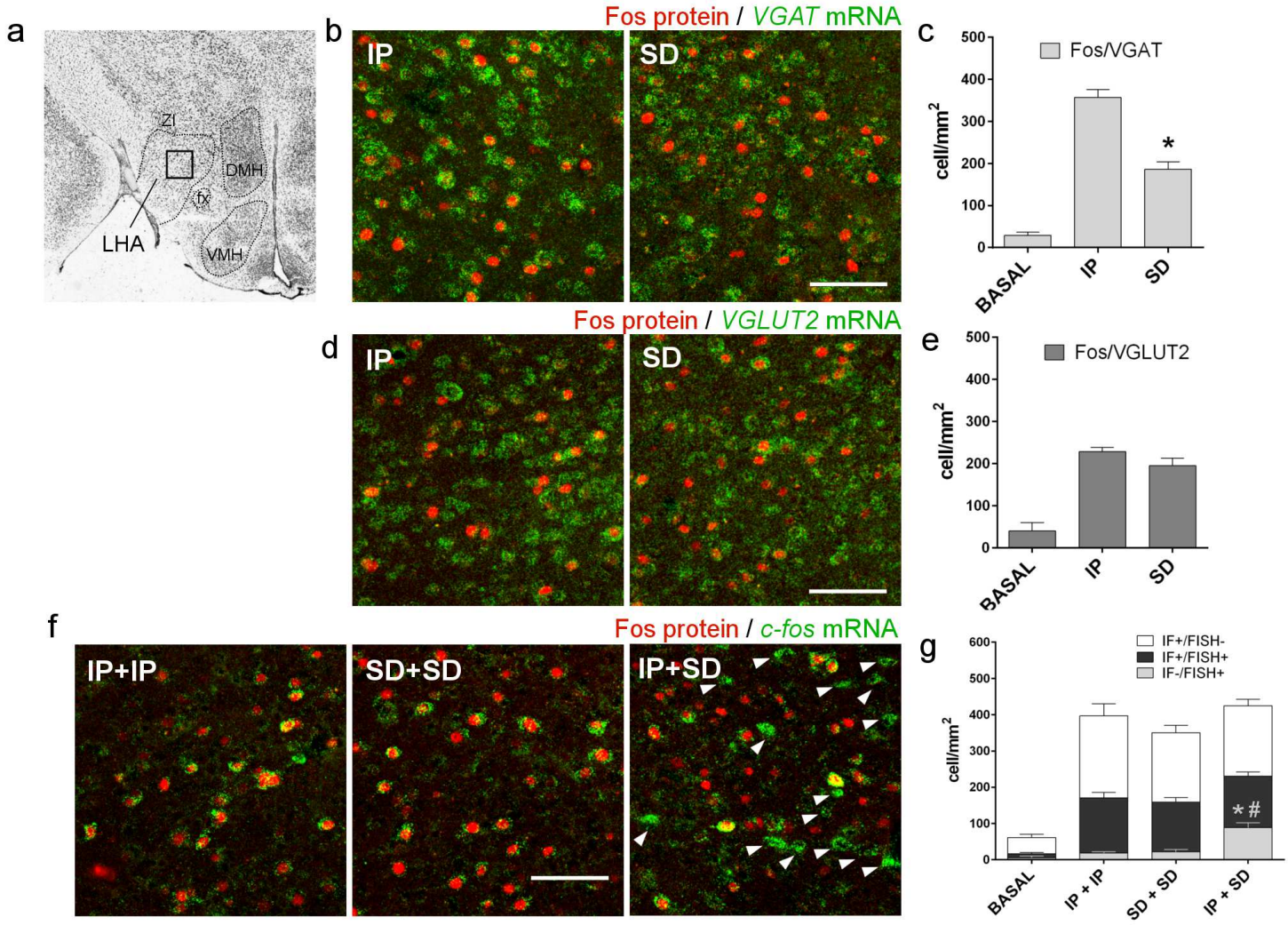

Figure 4

Analysis of the GABAergic and glutamatergic nature of LHA neurons recruited in response to predatory hunting and social defensive behavior and identification of LHA neural populations activated by IP and SD. a. Photomicrograph of a representative transverse thionin-stained section at tuberal levels of the LHA. Square-delineated region indicates the approximate location of higher magnification fluorescence photomicrographs showing Fos/VGAT and VGLUT2 mRNAs double labeling in (B) and (D). DMH – dorsomedial hypothalamic nucleus; fx – fornix; LHA – lateral hypothalamic area; ZI zona incerta. b, d. Representative fluorescence photomicrographs illustrating Fos protein/VGAT mRNA and Fos protein/VGULT2 mRNA double labeling in the LHA of animals exposed to IP and SD. Fos protein positive cells are labeled in red (Alexa 594) and VGAT mRNA positive cells are labeled in green (FITC). Scale bar, 75 µm. c, e. Median values of the density of Fos protein/VGATmRNA and Fos protein/VGULT2 mRNA double labeled cells in the BASAL (n = 3), IP (n = 6), and SD (n = 6) groups. SD group presented a lower number of Fos/VGAT mRNA neurons when compared to IP group (*p < 0.001). IP and SD groups did not differ in the number of Fos protein/VGLUT2 mRNA neurons. GzLM analysis followed with sequential Bonferroni corrections. Data are reported as mean ± SEM. f. Representative Fos protein/c-fos mRNA double labeling fluorescence photomicrographs of groups IP+IP, SD+SD, and IP+SD. Fos protein positive

cells are labeled in red (Alexa 594) and c-fos mRNA positive cells are labeled in green (FITC). Arrows indicate newly activated neurons (IF-/FISH+) in response to the second stimulus (SD). Scale bar, 75 µm. g. Median values of the density of IF+/FISH-, IF-/FISH+, and IF+/FISH+ neurons in the BASAL (n = 4), IP+IP (n = 4), SD+SD (n = 4), and IP+SD (n = 6) groups. Group IP+SD presented a higher number of newly activated neurons (IF−/FISH+) when compared to IP+IP (*p < 0.001) and SD+SD (#p < 0.001). GzLM analysis followed with sequential Bonferroni corrections. Data are reported as mean ± SEM.

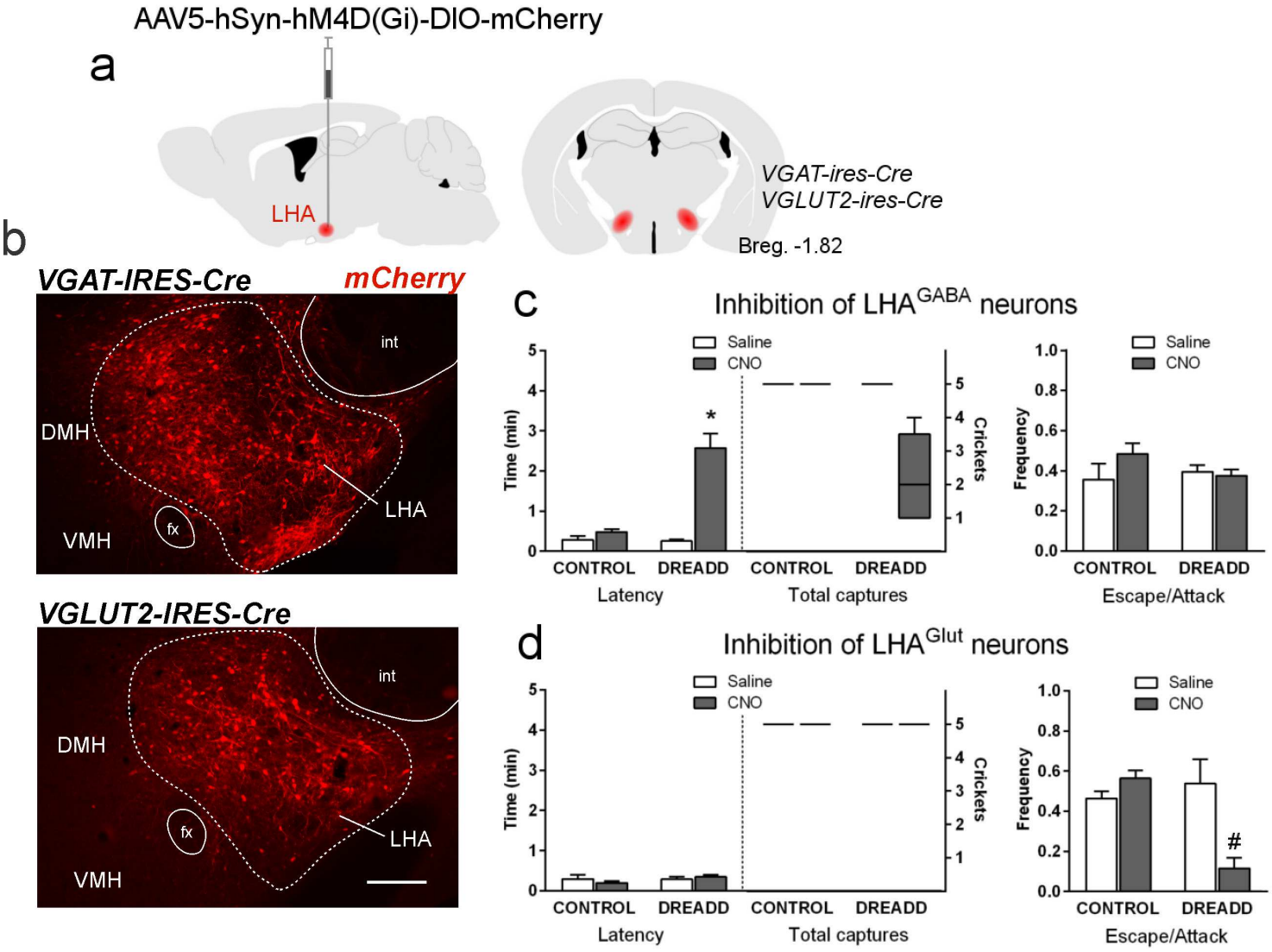

Figure 5

Functional role of LHAGABA and LHAGlut neurons on predatory hunting and social defensive behavior. a. Schematics showing the bilateral injection in the LHA of Cre-dependent AAV expressing hM4D inhibitory DREADD in VGAT-IRES-Cre and VGLUT2-IRES-Cre mice. b. Fluorescence photomicrographs showing neurons expressing mCherry (fused to HM4D) in the LHA of VGAT-IRES-Cre (top) and VGlut2-IRES-Cre (bottom) mice. DMH – dorsomedial hypothalamic nucleus; fx – fornix; int – internal capsule; LHA – lateral hypothalamic area; VMH – ventromedial hypothalamic nucleus. Scale bar, 200 µm. c. The effect of CNO-induced inhibition of LHAGABA neurons on predatory (latency to catch the first prey and total

number of captures; left) and social defensive (escape/attack ratio; right) behaviors. The data for latency and escape/attack ratio are shown as mean ± SEM, and the data for the number crickets captured are represented as box-whisker plots showing the median, interquartile range and minimum and maximum values. Groups: CONTROL (n = 5); DREADD (n = 9). 2 x 2 univariate ANOVAs for each dependent variable (latency to start hunting and escape / attack ratio) followed by Tukey's HSD test post hoc analysis (*p<0.001). d. The effect of CNO-induced inhibition of LHAGlut neurons on predatory (latency to catch the first prey and total number of captures; left) and social defensive (escape/attack ratio; right) behaviors. The data for latency and escape/attack ratio are shown as mean ± SEM, and the data for the number crickets captured are represented as box-whisker plots showing the median, interquartile range and minimum and maximum values. Groups: CONTROL (n = 5); DREADD (n = 5). 2 x 2 univariate ANOVAs for each dependent variable (latency to start hunting and escape / attack ratio) followed by Tukey's HSD test post hoc analysis (#p<0.01). See S6 – videos.

Supplementary Files

This is a list of supplementary files associated with this preprint. Click to download.

- FosDDCreIPSaline.mpg
- FosDDCreIPCNO.mpg
- FosDDCreSDSaline.mpg
- FosDDCreSDCNO.mpg
- WTIPLaseroff.mpg
- WTIPLaseron.mpg
- vGATLHAIPsaline.mpg
- vGATLHAIPCNO.mpg
- MarinBlascoetal2020Supplementarymaterial.pdf